

RESEARCH ARTICLE

SPECIAL ISSUE: CELL BIOLOGY OF THE IMMUNE SYSTEM

Myo1e modulates the recruitment of activated B cells to inguinal lymph nodes

Daniel A. Girón-Pérez, Eduardo Vadillo, Michael Schnoor and Leopoldo Santos-Argumedo*

ABSTRACT

The inclusion of lymphocytes in high endothelial venules and their migration to the lymph nodes are critical steps in the immune response. Cell migration is regulated by the actin cytoskeleton and myosins. Myo1e is a long-tailed class I myosin and is highly expressed in B cells, which have not been studied in the context of cell migration. By using intravital microscopy in an *in vivo* model and performing *in vitro* experiments, we studied the relevance of Myo1e for the adhesion and inclusion of activated B cells in high endothelial venules. We observed reduced expression of integrins and F-actin in the membrane protrusions of B lymphocytes, which might be explained by deficiencies in vesicular trafficking. Interestingly, the lack of Myo1e reduced the phosphorylation of focal adhesion kinase (FAK; also known as PTK2), AKT (also known as AKT1) and RAC-1, disturbing the FAK–PI3K–RAC-1 signaling pathway. Taken together, our results indicate a critical role of Myo1e in the mechanism of B-cell adhesion and migration.

KEY WORDS: Class I myosins, B cells, High endothelial venules, Adhesion, Migration

INTRODUCTION

The secondary lymphoid organs have a crucial role in immunity. Their distribution in the body allows the recruitment of immune cells upon encountering antigens (Mesin et al., 2016; Okada and Cyster, 2006; Pereira et al., 2010). The lymphocytes adhere to high endothelial venules (HEVs), which transport them to the lymph nodes, while recognizing various antigens. The adhesion and migration mechanisms are regulated by integrins, adhesins, chemokines and the actin cytoskeleton (Anderson and Anderson, 1976; Girard et al., 2012; Mionnet et al., 2011). The dysregulation of these molecules can alter the migration and recruitment of lymphocytes, thereby affecting the immune response. Therefore, the characterization of these molecules and investigation of their role might contribute to better understanding of the mechanism of migration.

Cell migration consists of various steps, which are highly regulated by signaling molecules (i.e. GTPases, kinases or motor proteins) (De Pascalis and Etienne-Manneville, 2017; Mayor and Etienne-Manneville, 2016; Mitchison and Cramer, 1996; Vicente-Manzanares et al., 2005) that control morphological changes needed for the movements of the cells (Mitchison and Cramer, 1996). These changes, modulated by alterations in the cytoskeleton, control the

extensions of the plasma membrane (Maravillas-Montero et al., 2011; Santos-Argumedo et al., 1997). Furthermore, during B-cell activation, the expression of integrins increases (Chigaev and Sklar, 2012; Laffón et al., 1991; Niggli et al., 1999; Wang et al., 2009), PI3K (Onishi et al., 2007) and GTPases are activated, and nucleation-promoting factors are recruited (Chen et al., 2012; Ma et al., 1998). Lipopolysaccharide (LPS)-mediated B-cell activation is increased upon the expression of the chemokine receptor CXCR4 (Brandes et al., 2000) and the adhesion molecules CD44 and LFA-1 (also known as Itgal) (Basit et al., 2006; Cannons et al., 2010; Hathcock et al., 1993).

Myosins are motor proteins belonging to 18 families (Thompson and Langford, 2002) and expressed in different tissues and organisms (Sellers, 2000). Class I myosins are single-head molecules that can bind to actin filaments and the plasma membrane (Osherov and May, 2000). The functions of class I myosins are associated with the regulation of motility and adhesion. Myo1e is highly expressed by macrophages, dendritic cells and B cells (Santos-Argumedo et al., 2013; Wenzel et al., 2015). In macrophages and dendritic cells, Myo1e interacts with ARF7EP (also known as AFR14EP) and participates in the antigen-presenting process (Paul et al., 2011). Myo1e may control the transport of major histocompatibility complex class II (MHC-II; also known as H2-Ab) to the plasma membrane in dendritic cells (Paul et al., 2011). Additionally, the lack of Myo1e in activated macrophages reduces their mobility (Tanimura et al., 2016). Intravital microscopy has shown the relevance of Myo1f in the extravasation, migration and deformation of the nucleus of neutrophils (Salvermoser et al., 2018), and in infections with *Listeria monocytogenes*, the motility of Myo1f-deficient neutrophils is reduced (Kim et al., 2006). The migration of activated B cells is important for their interaction with antigens in the inflammation sites (Zimmermann et al., 2019) or to travel to germinal centers (Mesin et al., 2016).

Here, we focused on the evaluation of Myo1e as a contributor to the migration of activated B cells. We report that the long-tailed Myo1e participates in activated B-cell adhesion to and slow rolling in HEVs of the inguinal lymph node. Through *in vitro* assays, we demonstrated that the absence of Myo1e results in reduced expression of integrins on the membrane of activated B cells. We provide evidence for the association of Myo1e with the PI3K–FAK–RAC-1 (FAK is also known as PTK2) signaling pathway. Thus, these results advocate for the critical participation of Myo1e in the process of migration and its possible functions in adhesion and extravasation regulation.


RESULTS

Absence of Myo1e results in inefficient recruitment of activated B cells to the inguinal lymph node

The recruitment of lymphocytes to the lymph nodes is a critical step in triggering an immune response. This process involves the rolling and adhesion of leukocytes to the HEVs (Kansas et al., 1993). We investigated whether Myo1e, expressed by B cells (Maravillas-

Departamento de Biomedicina Molecular, Centro de Investigación y de Estudios Avanzados del Instituto Politécnico Nacional, CP 07360, Mexico City, Mexico.

*Author for correspondence (lesantos@cinvestav.mx)

 D.A.G.-P., 0000-0001-5067-7464; E.V., 0000-0001-5939-8031; M.S., 0000-0002-0269-5884; L.S.-A., 0000-0002-4772-0713

Received 12 June 2019; Accepted 6 January 2020

Montero et al., 2011; Santos-Argumedo et al., 2013), affects their adhesion and motility to the HEVs. Therefore, the migration of activated B cells from wild-type (*Myo1e*^{+/+}) and *Myo1e*-deficient (*Myo1e*^{-/-}) mice was compared. Hoechst 33342-labeled B cells were injected into a host wild-type mouse and their adhesion and migration registered by intravital microscopy.

Different parameters of migration (adhesion, rolling and velocity) of activated B cells from *Myo1e*^{+/+} and *Myo1e*^{-/-} mice were compared. We monitored these parameters by intravital microscopy of the HEVs of the inguinal lymph node (IV to I) of a host wild-type mouse. An hour before inoculation, PBS (control) or CXCL12 was injected around the lymph node. Immediately after, activated B cells were injected into the carotid artery. The inguinal lymph nodes were exposed and the HEVs of the host mouse were evaluated using the parameters proposed by Von Adrian in 1996 (Von Adrian, 1996). We identified and numbered the HEVs from IV to I (Fig. S1).

Subsequently, the migration of activated B cells was monitored for 1 h in the different HEVs of the lymph node in the absence of any additional chemokines. We registered the adhesion and migration of B cells obtained from wild-type or *Myo1e*^{-/-} mice. In both situations, B-cell adhesion and migration in the PBS-inoculated mice was negligible (Movies 1 and 2, duration 00:29 s), while inguinal lymph node inoculated with CXCL12 showed reduced migration of *Myo1e*^{-/-} B cells when compared with B cells from *Myo1e*^{+/+} control mice (Movies 3 and 4, duration 00:29 s).

Myo1e is essential for the recruitment and adhesion of activated B cells to the inguinal lymph node

The recruitment of B cells in the absence of Myo1e was investigated in further detail. As can be seen in Fig. 1A and B, we counted the

numbers of activated B cells in HEVs IV to I of the inguinal lymph node of the host mice at different times (0, 30 and 45 min). We found a reduction in the recruitment of activated B cells from *Myo1e*^{-/-} mice, regardless of time. Additionally, we measured cell flow in the different HEVs (frequency of leukocytes that pass through the HEVs) at 1 min. We showed that the cell flow in HEVs I and II was increased in *Myo1e*^{-/-} B cells compared with control *Myo1e*^{+/+} B cells (Fig. 1C). To corroborate the previous results, we analyzed the numbers of activated B cells attached to the different HEVs for at least 15 s. We found reduced adherence of *Myo1e*^{-/-} B cells to HEVs III and IV (Fig. 1D). These results suggest that Myo1e modulates the migration of activated B cells into the inguinal lymph node.

The deficiency of Myo1e affects the speed and slow rolling of activated B lymphocytes

To characterize the motility of B lymphocytes, we measured the numbers of activated B cells performing rolling (velocity greater than 15 $\mu\text{m/s}$) in the different HEVs of the inguinal lymph node (IV to I). We found higher rolling of B cells from *Myo1e*^{-/-} mice traveling in HEVs IV and III compared with B cells from wild-type mice (Fig. 2A). In contrast, activated B cells from wild-type mice showed slow rolling (velocity less than 15 $\mu\text{m/s}$) (Weninger et al., 2000), indicating stronger attachment to the HEVs (Fig. 2B). Both measurements reflect an increase in the speed (relation between the distance and time that leukocytes move from HEV IV to I) of activated B cells from *Myo1e*^{-/-} mice compared with those from *Myo1e*^{+/+} mice (Fig. 2C). These results were corroborated when we measured the traveling time of activated B cells from HEV IV to I (Fig. 2D); B cells from *Myo1e*^{-/-} mice demonstrated higher velocity in comparison to B cells from the control mice. These results

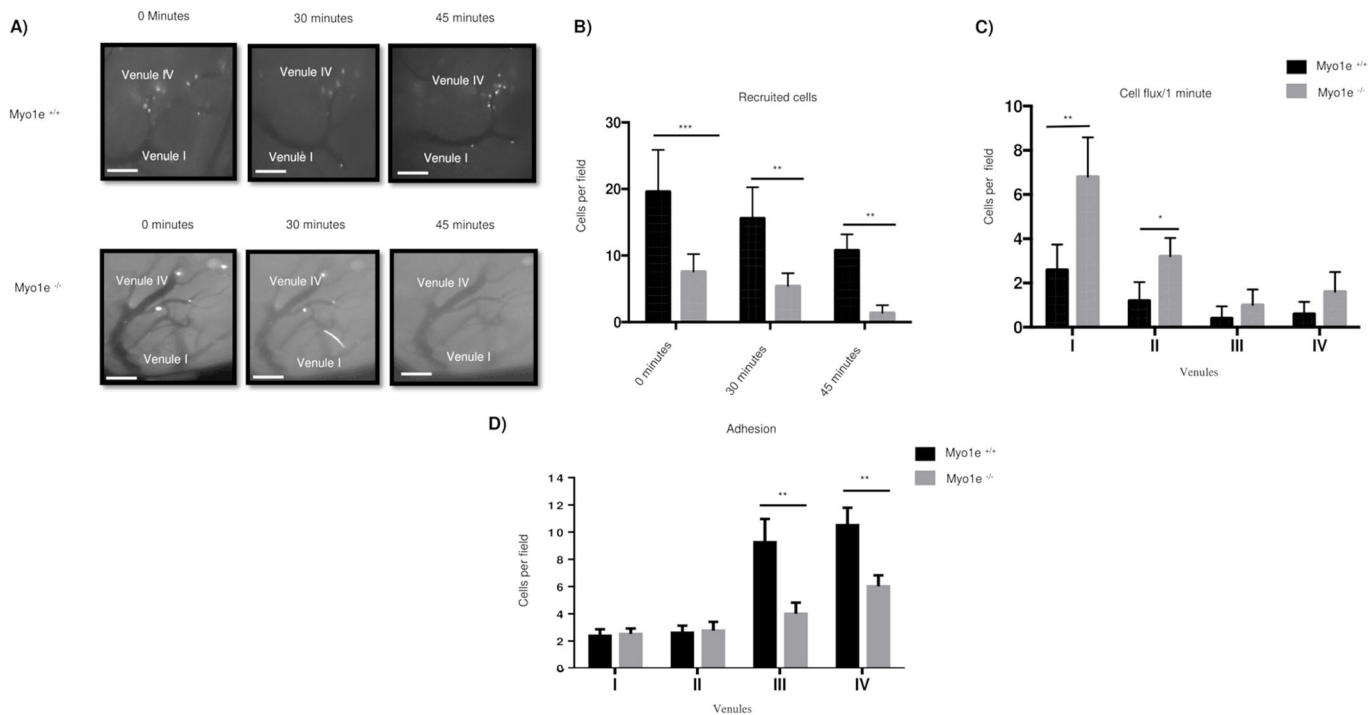


Fig. 1. Myo1e is required for recruitment and adhesion of activated B cells to the inguinal lymph node. (A) Representative images of intravital microscopy of activated B cells (stained with Hoechst 33342) from *Myo1e*^{+/+} and *Myo1e*^{-/-} mice inoculated in the HEVs of inguinal lymph node of a host *Myo1e*^{+/+} mouse. Images were captured (40 \times objective) at different time points (0, 30 and 45 min) in the HEVs of an inguinal lymph node that was injected with CXCL12 (25 ng/ml) or the vehicle (PBS) 1 h in advance. The HEVs were identified as IV to I. Scale bars: 25 μm ; $n=5$. (B) Quantification of recruited B cells at 0, 30 and 45 min. (C) Measurements of B cell flux (frequency of leukocytes that pass through the HEV) for 1 min. (D) Quantification of the adherent B cells in the different HEVs after 45 min, $n=5$. Data are presented as mean \pm s.d. * $P<0.05$, ** $P<0.01$, *** $P<0.001$.

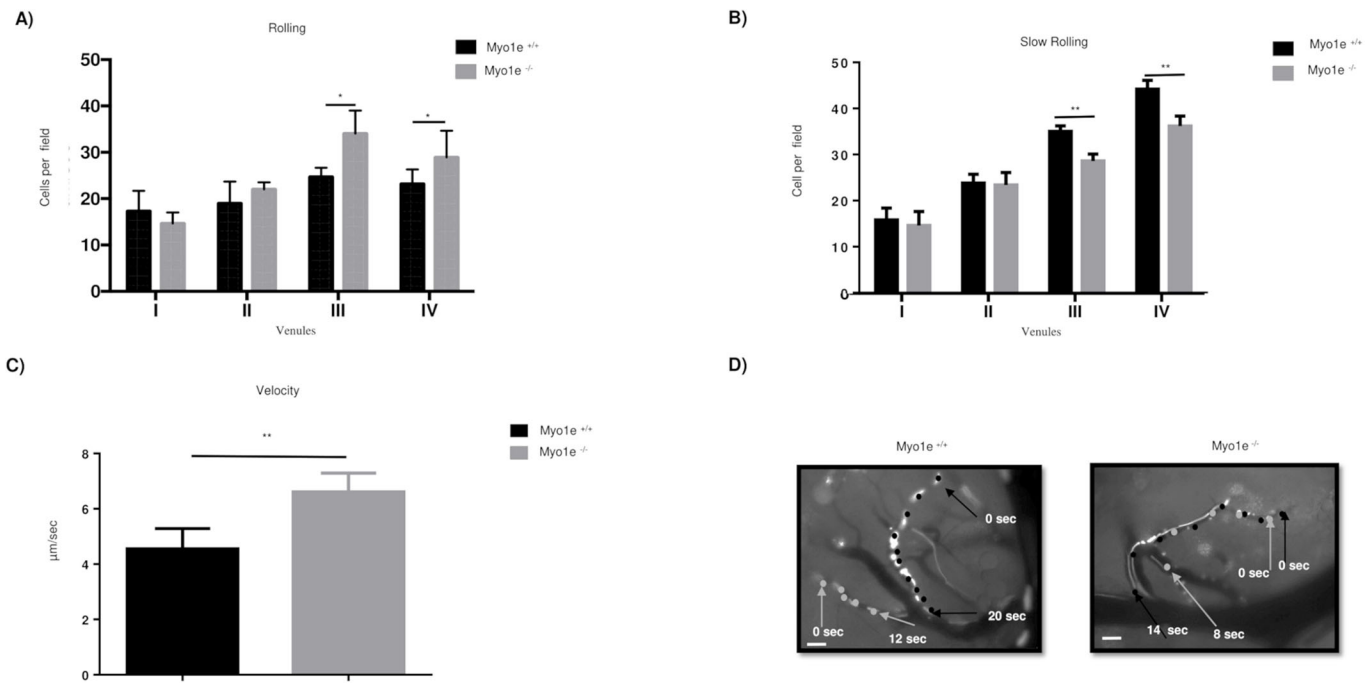


Fig. 2. The lack of *Myo1e* causes a reduction in the slow rolling and velocity of activated B lymphocytes. (A) Quantification of the activated B cells from *Myo1e*^{+/+} and *Myo1e*^{-/-} mice performing rolling (frequency of leukocytes with a rolling velocity greater than 15 $\mu\text{m/s}$) in the different HEVs (IV to I) of an inguinal lymph node of a host *Myo1e*^{+/+} mouse; $n=5$. Data are presented as mean \pm s.d. (B) Quantification of the activated B cells from *Myo1e*^{+/+} and *Myo1e*^{-/-} mice performing slow rolling (frequency of leukocytes with a rolling velocity less than 15 $\mu\text{m/s}$) in the different HEVs (IV to I) of an inguinal lymph node of a host *Myo1e*^{+/+} mouse; $n=5$. Data are mean \pm s.d. (C) Measurements of the velocity (traveling time from HEV IV to I) of activated B cells from *Myo1e*^{+/+} and *Myo1e*^{-/-} mice in the inguinal lymph node; $n=5$. Data are mean \pm s.d. (D) Representative images of the migration of activated B cells (stained with Hoechst 33342) from *Myo1e*^{+/+} and *Myo1e*^{-/-} mice inoculated in the HEVs of an inguinal lymph node of a host *Myo1e*^{+/+} mouse. The inguinal lymph node was injected with CXCL12 or vehicle (PBS) 1 h in advance. The arrows indicate the start of the route of B cells from HEV IV to I (40 \times objective). Scale bars: 25 μm ; $n=5$. * $P<0.05$, ** $P<0.01$.

indicate that *Myo1e* participates in the adherence and rolling of B lymphocytes to HEVs.

The absence of *Myo1e* in activated B cells affects their CXCL12-dependent homing to the inguinal lymph node

To corroborate our findings, homing assays were performed in which the right lymph node was inoculated with CXCL12, while the left lymph node was injected with the vehicle (Fig. S2A). Subsequently, carboxyfluorescein succinimidyl ester (CFSE)-labeled activated B cells from *Myo1e*^{+/+} and *Myo1e*^{-/-} mice were injected in different cell proportions into a host wild-type mouse. After 2 h, the host mouse was killed and CFSE-labeled B cells were recovered from blood, spleen, and right and left inguinal lymph nodes, and evaluated by flow cytometry. We found a reduction in the recruitment of *Myo1e*-deficient B cells in the right lymph node (Fig. S2B). Images from similar experiments were taken by intravital microscopy, and we counted all activated B cells (Hoechst 33342 labeled) recruited in the right or left inguinal lymph node (independently if they were from *Myo1e*^{+/+} or *Myo1e*^{-/-}). As can be seen, there were more cells recruited in the right lymph node responding to CXCL12 stimulation (Fig. S2C,D). We also found more *Myo1e*^{-/-} B cells recirculating in the blood and spleen, indicating that those cells were not recruited to the lymph nodes (Fig. S3). These findings demonstrate that *Myo1e* is a critical modulator of the migration and recruitment of activated B cells to the inguinal lymph node.

Myo1e modulates the chemotaxis of activated B lymphocytes

To analyze how the absence of *Myo1e* affects chemotaxis, the migration of activated B lymphocytes was evaluated in a Zigmond

chamber using CXCL12 as a chemoattractant. First, we stimulated with LPS+IL-4 at different time points (Fig. S4A,B), and found that, after stimulation for 48 h, *Myo1e*-deficient B cells showed reduced trajectories in comparison to B cells from wild-type control mice (Fig. 3A). This deficiency was also reflected in the direction ratio (angles that makes a straight line when changing directions) (Fig. 3B), Euclidean distances (straight-line distance between two points), accumulated distance (total distance traveled between two points) (Fig. 3C) and velocity (Fig. 3D). These results indicate the critical relevance of *Myo1e* in migration. We obtained the same result with anti-CD40+IL-4 stimulation (Fig. S4C,D). We also evaluated whether long-duration stimulation with LPS+IL-4 (48 h) differentiated B cells to plasmablasts. The results demonstrated that only a small percentage of activated B cells from *Myo1e*^{-/-} or *Myo1e*^{+/+} mice showed low expression of CD138 (also known as SDC1; a plasma cell differentiation molecule) (Fig. S4E).

Myo1e regulates the expression of integrins and adhesion molecules, affecting cell adhesion

Integrins and adhesion molecules modulate cell migration in different cells and tissues (Chuluyan and Issekutz, 1993; Gerberick et al., 1997; Manevich et al., 2007; Senbanjo and Chellaiah, 2017; Smith et al., 2003; Walling and Kim, 2018). These molecules allow the adherence of cells to the extracellular matrix, which serves as a support for the elongation of the membranes to generate the force needed for motility (Doyle et al., 2015; Francois et al., 2016; Sales et al., 2019). To further evaluate the defects in the motility of *Myo1e*-deficient B cells, we measured the relative amounts of LFA-1, CD44 and VLA-4 in activated B cells from *Myo1e*^{-/-} and *Myo1e*^{+/+} mice. Analysis of the mean fluorescence

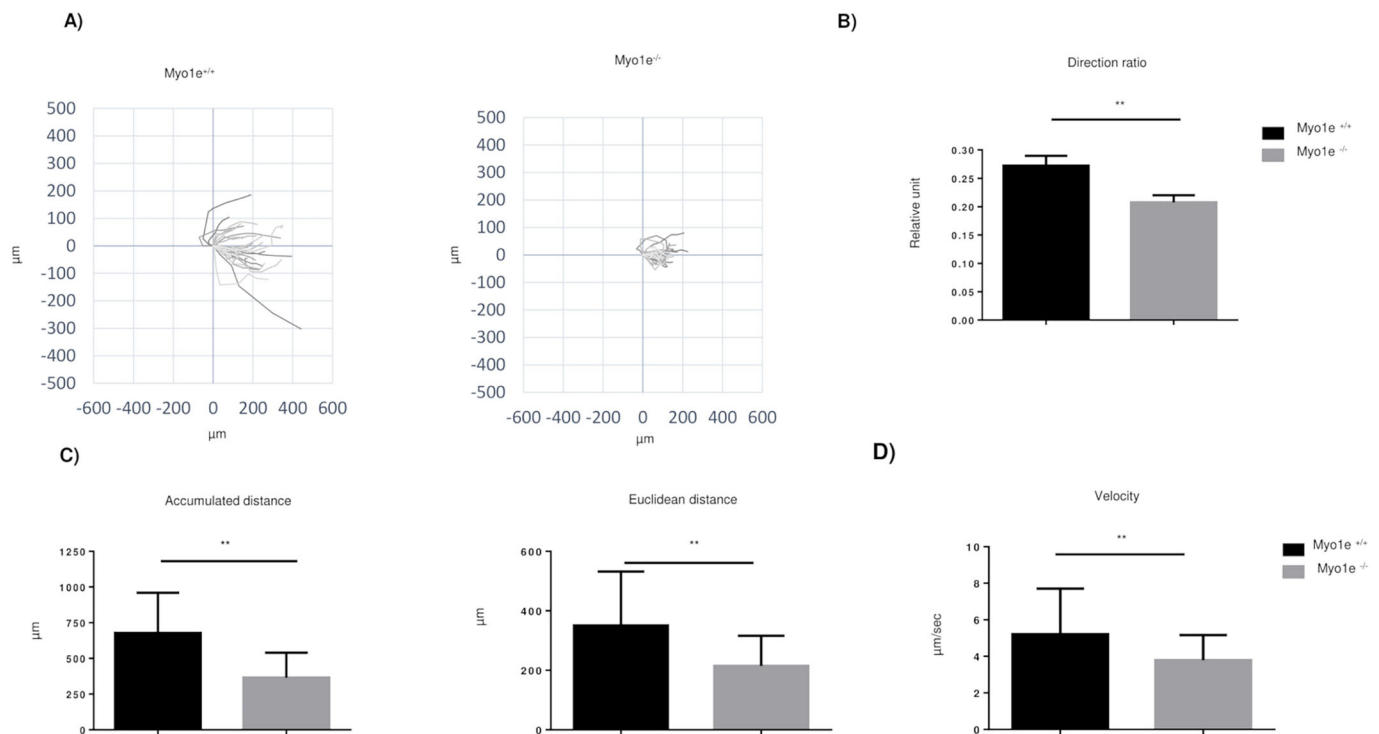


Fig. 3. The absence of *Myo1e* affects the distance and 2D motility of activated B cells in response to CXCL12. (A) Activated B cells from *Myo1e*^{+/+} and *Myo1e*^{-/-} mice were placed in a Zigmond chamber under a CXCL12 gradient and their migration was monitored for 1 h. Tracks of individual trajectories are presented in the plots; $n=5$. (B) Measurement of the direction ratio of migrating cells (angles that makes a straight line when changing directions). (C) Quantification of the accumulated (total distance traveled between two points) and the Euclidean distances (straight-line distance between two points). (D) Measurements of the velocity of activated B cells (under a CXCL12 gradient) from *Myo1e*^{+/+} and *Myo1e*^{-/-} mice; $n=5$. Data are presented as mean \pm s.d. ** $P < 0.01$.

intensity revealed reduced expression of these molecules in activated B cells from *Myo1e*^{-/-} mice compared to B cells from *Myo1e*^{+/+} mice (Fig. S5A,B). In order to corroborate these results, we performed adhesion assays using a monolayer of b.End3 cells (a brain endothelial cell line from SV129 mice). These cells have high expression of ICAM-1 and low expression of VCAM-1 on their surface. The results indicated that the reduction of integrins (LFA-1) to the surface of *Myo1e*-deficient B cells diminished their attachment to b.End3 cells (Fig. S5C).

Hoechst 33342-labeled B cells from *Myo1e*^{+/+} or *Myo1e*^{-/-} mice were allowed to adhere for 4 h and only the attached cells were further analyzed. Activated B cells from *Myo1e*^{-/-} mice showed reduced capacity of adhesion in comparison to B cells from *Myo1e*^{+/+} mice (Fig. S5D,E). These results suggest that *Myo1e* modulates cell migration through controlling the expression of LFA-1, CD44 and VLA-4 on the surface, and thereby the attachment of B cells to endothelial cells.

Cell transmigration and membrane protrusions requires the presence of *Myo1e*

Next, we evaluated the adhesion of B cells on specific substrates (fibronectin, hyaluronic acid, ICAM-1 and poly-L-Lysine as control). Activated B lymphocytes from *Myo1e*^{-/-} mice showed significantly reduced adherence to fibronectin, ICAM-1 and hyaluronic acid compared with B cells from *Myo1e*^{+/+} mice (Fig. 4A). Both classes of B cells did not show differences in their adhesion to a non-specific substrate like poly-L-Lysine. To extend these observations, we analyzed cellular transmigration through monolayers of b.End3 cells in transwell chambers. We found reduced transmigration of activated B cells when *Myo1e* was absent

(Fig. 4B). Interestingly, when measuring the membrane extensions of activated B cells, the cells from *Myo1e*^{-/-} mice exhibited reduced membrane protrusions (Fig. 4C,D). These observations are in line with the hypothesis of defective migration of B lymphocytes from *Myo1e*^{-/-} mice due to their reduced adhesion to the substrate.

The localization of integrins in the membrane protrusions is affected by the absence of *Myo1e*, and FAK is physically and functionally associated with *Myo1e*

To determine how *Myo1e* is involved in the signaling mediated by integrins, the pixel intensity of LFA-1 in the protrusion was measured. We found a lower signal intensity in the protrusions of activated B lymphocytes from *Myo1e*^{-/-} mice (Fig. 5A,B). The expression of CD44 and VLA-4 was also reduced in the membrane protrusions of *Myo1e*-deficient mice (Fig. S6A–D). In contrast, the expression of CXCR4 was not reduced (Fig. S7A,B). These results suggested that *Myo1e* is involved in vesicle trafficking of adhesion molecules.

Because FAK is a protein that plays a crucial role in integrin-mediated signal transduction, we investigated if there was an association between FAK and *Myo1e*. We also assessed FAK phosphorylation at tyrosine 397 in activated B cells that were stimulated for 15 min with CXCL12. The results showed that *Myo1e* co-immunoprecipitated with FAK. This interaction is stronger in activated than in resting B cells from *Myo1e*^{+/+} mice (Fig. 5C). Interestingly, FAK is phosphorylated at tyrosine 397 in activated B cells from *Myo1e*^{+/+} rather than from *Myo1e*^{-/-} mice, which were stimulated with CXCL12 (Fig. 5D,E). These results showed a physical and functional association between FAK and *Myo1e*, suggesting that *Myo1e* is involved in the signaling pathway of integrins.

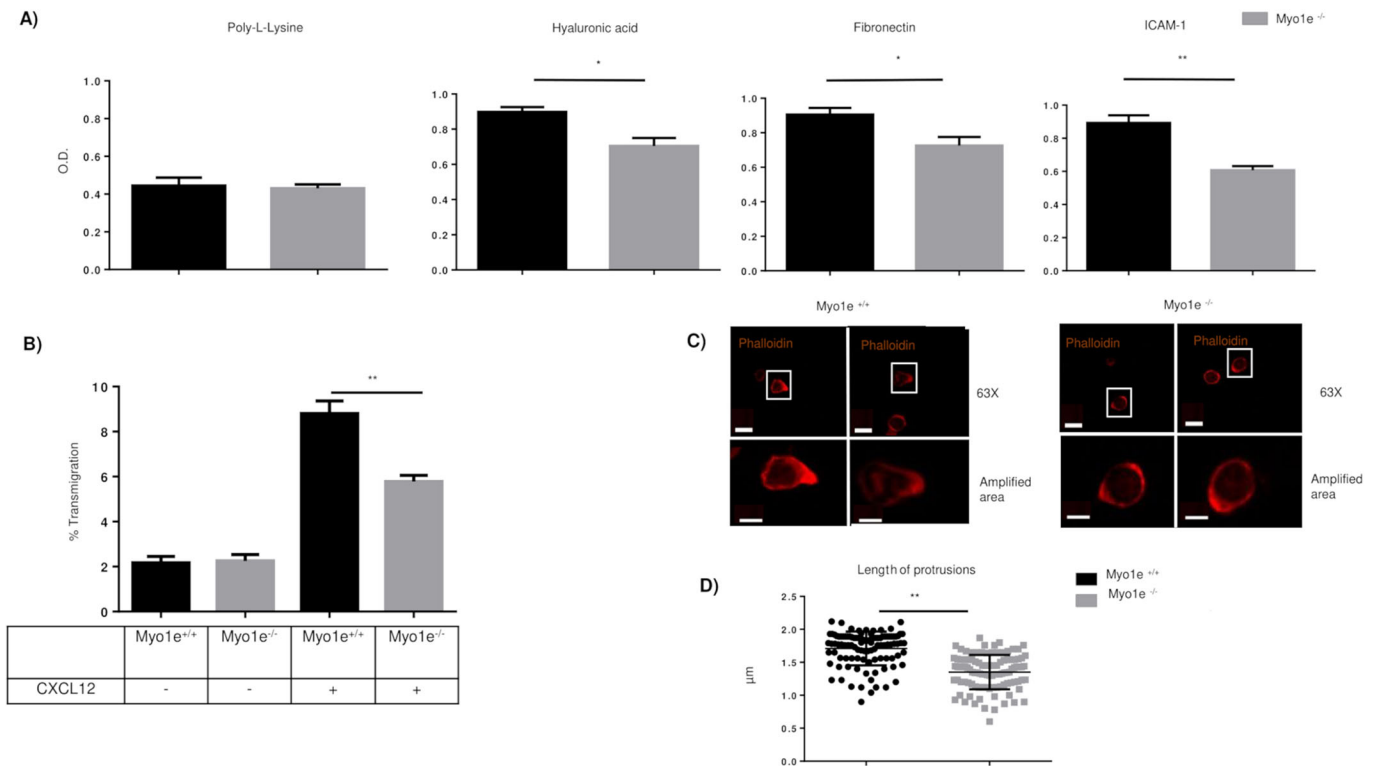


Fig. 4. The deficiency of Myo1e affects the transmigration and length of protrusions of the membrane of activated B cells. (A) One hundred thousand activated B cells from *Myo1e*^{+/+} and *Myo1e*^{-/-} mice were placed into each well in a 96-well plate. Previously, the plate was coated with hyaluronic acid, ICAM-1, fibronectin or poly-L-lysine for 2 h, then the wells were washed and the cells adhered to the wells were stained with Crystal Violet. Finally, the cells were lysed and the absorbance of the Crystal Violet was determined at 590 nm; *n*=3. Data are mean±s.d. (B) Activated B cells from *Myo1e*^{+/+} and *Myo1e*^{-/-} mice were seeded on top of a confluent monolayer of bEnd.3 cells in a transwell chamber. The migration of activated B cells was stimulated by a gradient of CXCL12 or vehicle, both in RPMI medium. After 4 h, migrating B cells were recovered from the bottom chamber and quantified by flow cytometry. Percentages of transmigration are presented in the graph; *n*=3. Data are presented as mean±s.d. (C) Representative images (63× objective) of activated B cells (under a gradient of CXCL12) from *Myo1e*^{+/+} and *Myo1e*^{-/-} mice. Scale bars: 5 μm (amplified area, zoom 2.5); *n*=3. (D) Measurement of the length of protrusions of activated B cells from *Myo1e*^{+/+} and *Myo1e*^{-/-} mice. Data are presented as mean±s.d. **P*<0.05, ***P*<0.01.

Myo1e interacts with CARMIL, affecting the polymerization of actin in the membrane protrusions

We evaluated the polymerization of actin in the protrusions of migrating CXCL12-activated B lymphocytes. We found a reduction in F-actin at the leading edge of the membrane of B cells lacking Myo1e (Fig. S7C,D).

CARMIL is a family of proteins involved in the migration of the cells. The potential interaction of CARMIL with Myo1e was analyzed via colocalization (Fig. S7E,F) and co-immunoprecipitation (Fig. S7G) assays. Both methods showed that Myo1e and CARMIL proteins are interacting at the leading edge of migrating B lymphocytes. These results indicate that Myo1e participates in the remodeling of filamentous actin at the leading edge of migrating activated B lymphocytes.

Myo1e deficiency decreases cellular spreading, activity of RAC-1 and phosphorylation of AKT

The Rho family of small GTPases is a key regulator of the actin cytoskeleton, thereby controlling the activity of numerous downstream effectors. RAC-1, a member of the Rho family, together with AKT (a serine/threonine kinase; also known as AKT1) participate in actin reorganization required for the formation of protrusions during adhesion, spreading and motility of cells. Thus, we evaluated cellular spreading by measuring the curvature of the cell. A ratio of semi-major versus semi-minor axis

(elliptical factor) ≤ 2 is indicative of the polarized morphology of cells. Most B cells from *Myo1e*^{-/-} mice had an elliptical factor < 2 (Fig. 6A,B).

The evaluation of RAC-1 in activated B cells from Myo1e-deficient mice demonstrated reduced activity of this GTPase (Fig. 6C,D). Similarly, the phosphorylation of AKT at threonine 308 was reduced in these lymphocytes when they were stimulated for 15 min with CXCL12 (Fig. 6E,F). These results reveal the relevance of Myo1e in the activity of actin-related proteins such as GTPase RAC-1 and AKT (Henderson et al., 2015; Niba et al., 2013; Zhu et al., 2015).

Myo1e participates in controlling the migration of B lymphocytes through the PI3K-AKT-RAC-1 signaling pathway

The regulation of AKT and RAC-1 is dependent on the activation of PI3K. Both enzymes are needed for F-actin-driven elongation of the membrane at the leading edge. By using a PI3K inhibitor, LY294002, we found a decrease in elongation and reduced F-actin at the leading edge. The results strongly resemble those seen with Myo1e-deficient activated B cells (Fig. 7A–C). These results correlate with the reduction in FAK phosphorylation at tyrosine 397, AKT phosphorylation at threonine 308, and RAC-1 activity (Fig. 7D,E). Taken together, these results strongly suggest that Myo1e is critical for cell migration and integrin activation. The FAK-AKT-RAC-1 signaling pathway requires the participation of Myo1e.

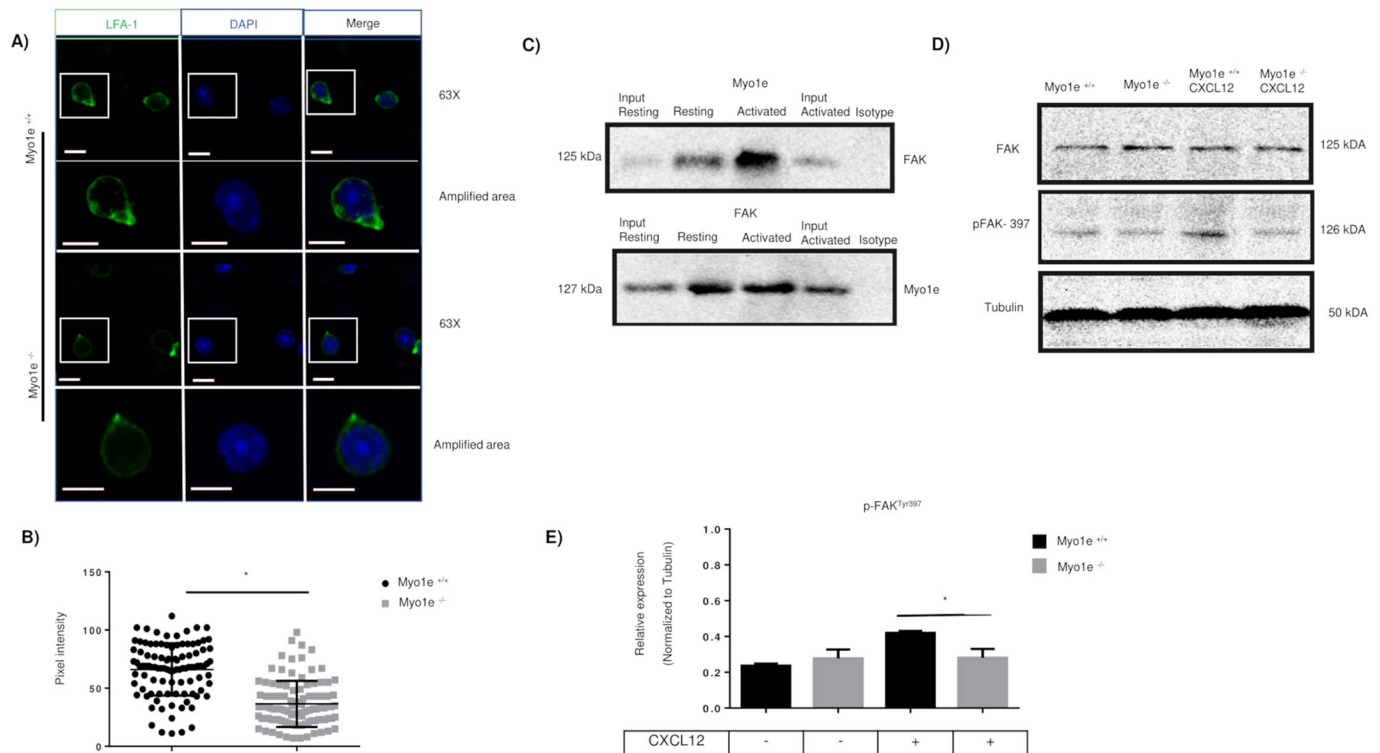


Fig. 5. Myo1e interacts with FAK and the lack of Myo1e causes a reduction in the localization of integrins. (A) Representative images (63× objective) of B cells activated under a CXCL12 gradient from *Myo1e*^{+/+} and *Myo1e*^{-/-} mice. The cells were stained with anti-LFA-1 (green) and 4',6-diamidino-2-phenylindole (DAPI; blue). Scale bars: 5 μm (amplified area, zoom 2.5); *n*=3. (B) The intensity of pixels in the protrusions of the membrane of activated B cells from *Myo1e*^{+/+} and *Myo1e*^{-/-} mice was measured; *n*=3. Data are presented as mean±s.d. (C) Co-immunoprecipitation of Myo1e with FAK in resting and activated B cells; *n*=3. (D) Representative western blot analysis of the tyrosine 397 phosphorylation of FAK in activated B cells with or without stimulation with CXCL12; *n*=3. (E) Densitometric analysis of FAK phosphorylation at tyrosine 397 (normalized to tubulin); *n*=3. Data are presented as mean±s.d. **P*<0.05.

DISCUSSION

Class I myosins have been involved in the regulation of adhesion, motility and recycling of receptors through the transport of vesicles and the interaction with different cytoskeletal proteins (López-Ortega and Santos-Argumedo, 2017; Maravillas-Montero et al., 2011; Piedra-Quintero et al., 2019). However, only a few studies have analyzed the participation of class I myosins in the signaling of leukocytes during cell migration (López-Ortega et al., 2016; Salvermoser et al., 2018). In the present study, we used intravital microscopy and demonstrated the relevance of Myo1e in the motility of activated B cells. The absence of Myo1e suppresses the recruitment of activated B cells to the inguinal lymph nodes. This reduction is accompanied by a decrease in slow rolling and adhesion in HEVs (IV and III). Similar results were reported regarding Myo1f-deficient neutrophils, which displayed reduction in spreading, transmigration and extravasation in cremasteric venules. This deficiency is due to alterations in the morphology of the cells that prevent their correct adhesion, and thereby their transmigration through tight junctions. However, the mechanism of action is not completely resolved (Salvermoser et al., 2018). Additionally, other studies have shown the role of integrins in leukocyte migration. A video-microscopy analysis in Peyer's patches showed a reduction in the recruitment and adhesion of lymphocytes when they were treated with neutralizing antibodies against LFA-1 or the α4 subunit of integrins (Bargatze et al., 1995).

The reduced recruitment of activated B cells to HEVs was confirmed by homing assays, in which we observed that the absence of Myo1e causes a reduction in the recruitment of B cells in the

inguinal lymph node, concomitant with an accumulation in the blood and spleen (Ager, 2017; Nolte et al., 2002). This defect might be explained by the observed reduction in integrin expression.

Of note, the role of Myo1e in motility was only detected in activated B cells and no significant differences were found in resting B cells in response to CXCL12 (data not shown). Activated B cells from Myo1e-deficient mice had reduced 2D migration, decreased adherence to ICAM-1, fibronectin and hyaluronic acid, and diminished adherence to monolayers of bEnd.3 cells. Additionally, we found shortened membrane protrusions in Myo1e-deficient activated B cells.

Migration is modulated by the expression of integrins. Integrin expression increases upon cellular activation (Chung et al., 2014) and chemokine receptor stimulation (Goichberg et al., 2006; Takabayashi et al., 2009). Furthermore, integrins are critical for the rearrangement of the cytoskeleton. Through different signaling pathways, these proteins contribute to the generation of membrane projections, which act as anchors supporting the force needed for motility (Hood and Cheresch, 2002; Kritikou, 2008). Our results revealed that the absence of Myo1e in activated B lymphocytes causes a decrease in the expression of LFA-1, CD44 and VLA-4 in the membrane protrusions of these cells.

The activation of B cells by different stimuli causes the activation of different molecules such as FAK, PI3K, AKT, PLCγ2, Fyn and RAC-1. This process involves changes in the cytoskeletal reorganization, increase in lateral mobility, and clustering of VCAM-1 and LFA-1. The reorganization of these molecules does not occur in resting B cells (Spaargaren et al., 2003). Cell adhesion is affected by the clustering of integrins, and the enhancement of

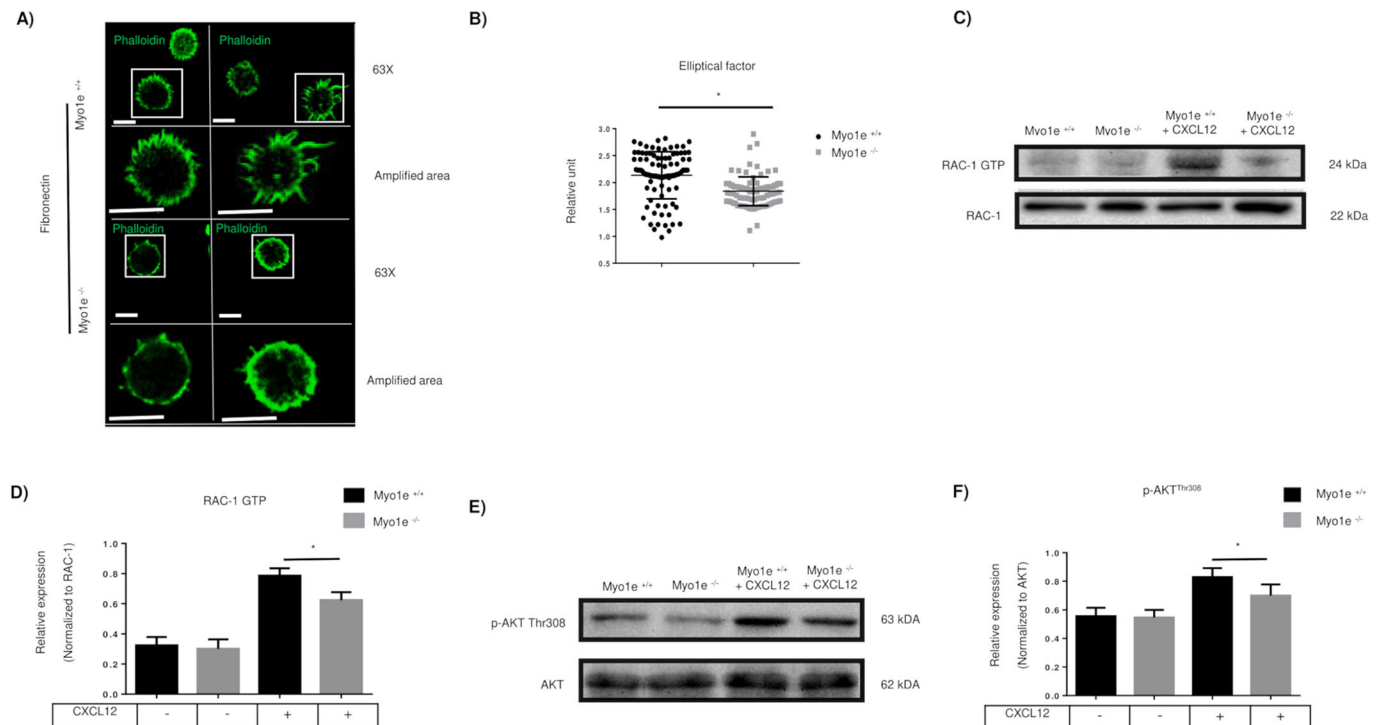


Fig. 6. *Myo1e* is critically required for spreading and requires activation of the AKT–RAC-1 pathway. (A) Representative images (63× objective) of activated B cells from *Myo1e*^{+/+} and *Myo1e*^{-/-} mice. B cells were seeded to spread over fibronectin for 1 h, followed by staining with TRITC-Phalloidin. Scale bars: 5 μm (amplified area, zoom 2.5); *n*=3. (B) Quantification of the elliptical factor (ratio of semi-major versus semi-minor axis) in B cells from *Myo1e*^{+/+} and *Myo1e*^{-/-} mice; *n*=3. Data are presented as mean±s.d. (C) Representative western blot analysis of the active form of RAC-1 in activated B cells from *Myo1e*^{+/+} and *Myo1e*^{-/-} mice, with or without stimulation with CXCL12; *n*=3. (D) Densitometric analysis of the RAC-1–GTP activity (normalized to RAC-1); *n*=3. Data are presented as mean±s.d. (E) Representative western blot for assessing AKT phosphorylation at threonine 308 in activated B cells from *Myo1e*^{+/+} and *Myo1e*^{-/-} mice, with or without stimulation with CXCL12; *n*=3. (F) Densitometric analysis of AKT phosphorylation at threonine 308 (normalized to AKT); *n*=3. Data are presented as mean±s.d. **P*<0.05.

affinity and avidity of the adhesion molecules to diverse substrates (Spaargaren et al., 2003).

The integrin clusters promote the auto-phosphorylation of FAK at tyrosine 397 (Calalb et al., 1996) and allow the recruitment of paxillin (Hu et al., 2014), tensin (Qian et al., 2009) and talin (Nader et al., 2016), which form a complex that stabilizes adhesion. Our results obtained in B cells confirm the interaction between FAK and *Myo1e* in B cells, which has been previously reported in WM858 melanoma cells (Heim et al., 2017). This interaction promotes the auto-phosphorylation of FAK upon stimulation with CXCL12 in activated B cells. Studies in DU-145 cells (human epithelial cells) using hematopoietic precursors have demonstrated that CXCL12 increases the phosphorylation of FAK and the expression of β3 and α5 integrins, which then contributes to the adhesion mediated by VCAM-1 (Engl et al., 2006; Glodek et al., 2007). Therefore, we hypothesize that *Myo1e* is responsible for carrying FAK towards the integrin, allowing FAK auto-phosphorylation and formation of a complex, which is necessary for efficient cell adhesion and motility.

The membrane protrusions are important morphological structures for motility and protein localization (Tanaka et al., 2017; Xue et al., 2010). The interaction of *Myo1e* with CARMIL proteins is critical for the formation and elongation of actin filaments (Liang et al., 2009). In this work, we demonstrated the interaction of CARMIL proteins with *Myo1e* in activated B cells. These results suggest that, under *Myo1e* deficiency, CARMIL proteins are not recruited to the membrane, causing reduction in the membrane extensions.

Spreading is a mechanism used by cells to maximize the contact area with different ligands. This is an essential step for slow rolling

and cellular transmigration. Deficiency in spreading has been described as a disturbance in the integrity of the cytoskeleton (Kim and Wirtz, 2013; Wakatsuki et al., 2003). In our work, we showed that *Myo1e* deficiency causes a reduction in spreading, indicating that *Myo1e* is also involved in cell deformation.

RAC-1 is an essential small GTPase involved in the formation of actin filaments, spreading and cell motility. Its deficiency in mouse embryonic fibroblasts (MEFs) caused a reduction in the activity of RAC-1, altering cell morphology (Chang et al., 2011). This phenomenon has also been reported in HeLa cells, in which Rac-1 activity is inhibited in the absence of RAP1, altering cell spreading and motility (Arthur et al., 2004).

The phosphorylation of AKT at threonine 308 regulates the activity of RAC-1 through PDK1 (Higuchi et al., 2008; Liu et al., 2018; Niba et al., 2013). An increase in the activity of RAC-1 and in the phosphorylation of AKT by stimulation with growth factors has also been reported in MDA-MB-231 mammary gland epithelial cells treated with epidermal growth factor (Yang et al., 2011). Our results show a decrease in the spreading of activated B lymphocytes from *Myo1e*^{-/-} mice, which correlates with reduced activity of RAC-1 and reduced phosphorylation of AKT at threonine 308. FAK phosphorylates PI3K, an enzyme involved in the conversion of phosphatidylinositol 4,5-bisphosphate (PIP2) to phosphatidylinositol 3,4,5-triphosphate (PIP3) in the membrane (Agelaki et al., 2007; Matsuoka et al., 2012). PIP3 anchors AKT at the membrane and promotes the activity of RAC-1. Suppression of the FAK–PI3K–RAC-1 pathway in the EA.hy926 cell line (human endothelial cells) and the MCF7 cell line (human epithelial cells) decreases cell

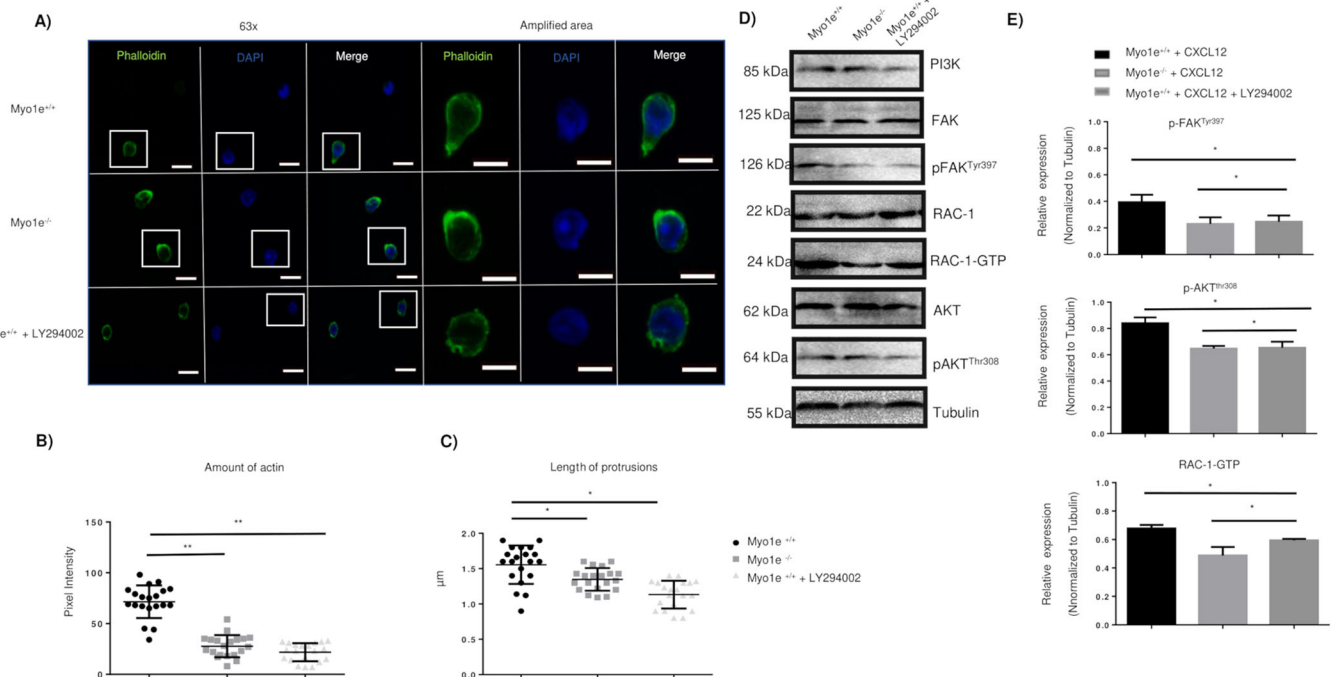


Fig. 7. The inhibition of PI3K affects the protrusions of the membrane of activated B cells. (A) Representative images (63× objective) of CXCL12-activated B cells from *Myo1e*^{+/+} or *Myo1e*^{-/-} mice and B cells from *Myo1e*^{+/+} pretreated with LY294002 for 1 h. Scale bars: 5 μm (amplified area, zoom 2.5); *n*=3. (B) Pixel intensity in the protrusions of the membrane of CXCL12-activated B cells from *Myo1e*^{+/+} or *Myo1e*^{-/-} mice and LY294002-pretreated B cells from *Myo1e*^{+/+} mice; *n*=3. Data are presented as mean±s.d. (C) Length of the protrusions of the membrane in CXCL12-activated B cells from *Myo1e*^{+/+} or *Myo1e*^{-/-} mice and in LY294002-pretreated B cells from *Myo1e*^{+/+} mice; *n*=3. Data are presented as mean±s.d. (D) Representative western blot of PI3K, p-AKT (Thr308) and p-FAK (Tyr397) phosphorylation and activity of RAC-1 in CXCL12-activated B cells from *Myo1e*^{+/+} or *Myo1e*^{-/-} mice and LY294002-pretreated B cells from *Myo1e*^{+/+} mice. (E) Densitometric analysis of the expression of RAC-1-GTP, p-AKT (Thr308) and p-FAK (Tyr397) (normalized to tubulin) in CXCL12-activated B cells from *Myo1e*^{+/+} or *Myo1e*^{-/-} mice and LY294002-pretreated B cells from *Myo1e*^{+/+} mice; *n*=3. Data are presented as mean±s.d. All data shown are representative of three independent experiments. **P*<0.05, ***P*<0.01.

migration (Huang et al., 2013; Kallergi et al., 2007). We found that, in the absence of *Myo1e*, activated B cells stimulated with CXCL12 behave similarly to wild-type B cells inhibited by LY294002 (a PI3K inhibitor), suggesting the functional interaction of these molecules in the adhesion and migration of activated B lymphocytes. These results were corroborated by the reduced phosphorylation of FAK and AKT and the suppressed activity of RAC-1. Taken together, these results indicate that *Myo1e* is involved in the FAK–PI3K–RAC-1 signaling pathway.

PI3K mediates cell adhesion by modulating the conversion of phospholipids (PIP2 to PIP3) in the membrane, allowing the formation of clusters of integrins and triggering the signaling for actin polymerization. *Myo1e* is enriched at podosomes and is anchored at the plasma membrane in a PIP3-dependent manner, as demonstrated in MEFs, in which PTEN and SHIP2 (also known as INPPL1) phosphatases were overexpressed and caused a reduction in the recruitment of *Myo1e* to this structure (Zhang et al., 2019).

The TH1 and TH2 domains of *Myo1e* facilitate the interaction with membrane phospholipids. Mutations in these domains (K772A and R782A) were shown to reduce the *Myo1e* binding affinity for PIP3 and to suppress the actin polymerization in the podosomes of MEFs. This result suggests that *Myo1e* may participate in the recruitment of nucleation-promoting factors to the plasma membrane (Zhang et al., 2019). Our results reveal that PI3K inhibition by LY294002 results in reduced filamentous actin in the membrane protrusions and suppressed cell spreading.

Cellular activation leads to reorganization of the actin cytoskeleton, increased expression of integrins, increased chemokine receptor expression, phosphorylation of diverse molecules, exchange of

phospholipids in the membrane and lateral mobilization of molecules for the formation of clusters. All these changes are necessary for efficient adhesion and migration of cells. In resting B cells, the changes are minimal or do not occur at all. Therefore, the absence of *Myo1e* in resting B cells did not result in defects in adhesion and migration in response to CXCL12. Resting B cells mainly respond to CXCL13 stimulation. Our preliminary results have shown deficient migration of resting B lymphocytes from *Myo1e*^{-/-} mice in response to this stimulus (data not shown).

The preliminary characterization of *Myo1e*^{-/-} mice suggests that these animals lack major defects in their immune response. However, it is worth mentioning that all experiments have been performed in a non-infectious and controlled environment. Therefore, a future perspective in the field is to evaluate *Myo1e*-deficient mice challenged with infectious agents, a work that is in progress in our laboratory.

In conclusion, we have presented evidence that *Myo1e* is critical for the recruitment and adhesion of activated B cells to the inguinal lymph node through the localization of integrins, and that this phenomenon is modulated by the FAK–PI3K–RAC-1 signaling pathway.

MATERIALS AND METHODS

Mice and reagents

In all experiments, we used female C57BL/6J or B6.129S6(Cg)-*Myo1e*^{em1.1FtvjJ} mice (8–10 weeks old). The mice, kindly provided by Dr Richard Flavell (Yale School of Medicine, New Haven, CT), were bred and maintained in the animal facility at Centro de Investigación y de Estudios Avanzados (CINVESTAV) (Mexico City, Mexico). This study was carried out in strict accordance with ARRIVE (Animal research: reporting of

in vivo experiments) and the Animal Care and Use Committee at CINVESTAV approved all protocols and experiments.

All mice were provided with free access to water and a diet containing 20% protein (PicoLab[®] mouse diet 20, LabDiet[®] 5058, St Louis, MO). A 12-h light/dark cycle, room temperature of 22±2°C and humidity at 50±10% were used. All cages contained Aspen chips and Aspen shavings (50/50%) (NEPCO[®], Warrensburg, NY) as bedding. Moreover, they included wood shavings, bedding and a cardboard tube for environmental enrichment.

Lymphocyte isolation and flow cytometry

Splenic mononuclear cells were isolated by Ficoll-paque Plus (GE Healthcare, Little Chalfont, UK) density gradient separation, and B220⁺ cells were enriched by panning, using plastic dishes coated with α -Thy-1 monoclonal antibody ascites (NIM-R1) (Chayen and Parkhouse, 1982).

For B-cell activation, 2×10⁶ cells were incubated for 48 h at 37°C and 5% CO₂ in 1 ml RPMI 1640 (Life Technologies, Grand Island, NY) supplemented with 10% fetal bovine serum (Thermo Fisher Scientific, Waltham, MA), LPS from *Escherichia coli* O55:B5 at 20 µg/ml (Sigma-Aldrich, St Louis, MO), or anti-CD40 at 10 µg/ml (Santa Cruz Biotechnology, Dallas, TX) and 10 U/ml IL-4 (R&D Systems, Minneapolis, MN).

For immunostaining, we blocked the Fc receptors using 10% goat serum. The cell suspensions were immediately washed with PBS containing 1% bovine serum albumin (BSA) (Thermo Fisher Scientific) and 0.01% NaN₃ (PBA). One million cells were stained for 15 min using the antibodies described in the following section. After incubation, the cells were washed with PBA and fixed with 1% formaldehyde in PBS (0.5% albumin, 0.01% NaN₃, 100 ml PBS). The doublets were excluded with the gating on FSC-H versus FSC-A, and the lymphocytes were identified by their scatter properties (FSC-A versus SSC-A). Compensation was performed using single-stained cells for each of the fluorochromes used. The cells were evaluated using a BD LSR Fortessa flow cytometer (Becton-Dickinson, San Jose, CA) and analyzed using FlowJo v.10 software (Tree Star, Ashland, OR). All experiments were performed according to the flow cytometry guidelines (Cossarizza et al., 2017).

Antibodies and reagents

The antibodies used in this study were: anti-B220-BV421 (clone RA3-6B2, cat# 103239, dilution 1:500, BioLegend, San Diego, CA), anti-B220-Alexa Fluor 488 (clone RA3-6B2, cat# 103228, dilution 1:200, BioLegend), anti-CD19 (clone 6D5, cat# 1575-09L, dilution 1:300, Southern Biotechnology Associates, Birmingham, AL), anti-CD29 (clone HMβ1-1, cat# 102201, dilution 1:500, BioLegend), anti-LFA-1 (clone H155-78, cat# 141009, dilution 1:1000, BioLegend), anti-CD62L (clone DREG-56, cat# 304816, dilution, 1:400, BioLegend), anti-TLR-4 (clone TF901, cat# BDB564215, dilution 1:1000, BioLegend), anti-CXCR4 (clone L276F12, cat# 146502, dilution 1:100, BioLegend), anti-CD44 (clone IM7, cat# 103023, dilution 1:1000, BioLegend), anti-Myo1e (clone PAD434, cat# PAD434Mu01, dilution 1:300, Cloud Corp, Katy, TX), anti-CARMIL (clone E-10, cat# sc-365314, dilution 1:400, Santa Cruz Biotechnology), anti-WASp (clone EP2541Y, cat# ab75830, dilution 1:250, Abcam, Cambridge, UK), anti-RAC-1 (clone c-11, cat# sc-95, dilution 1:500, Santa Cruz Biotechnology), anti-RAC-1 GTP (clone 26903, cat# NB-26903, dilution 1:300, ser-61, Biomol, Hamburg, Germany), anti-PI3K (clone B-9, cat# sc-1637, dilution 1:300, sc-1637, Santa Cruz Biotechnology), anti-CD40 (clone HM40-3, cat# sc-20010, dilution 1:200, Santa Cruz Biotechnology), anti-CD138 (clone 281-2, cat# 142505, dilution 1:400, Santa Cruz Biotechnology), anti-AKT (clone B-1, cat# sc-5298, dilution 1:500, Santa Cruz Biotechnology) and anti-phospho-AKT (clone B-5, cat# sc-271966, dilution 1:400, Santa Cruz Biotechnology). Other reagents used throughout the study include TRITC-Phalloidin (cat# R415, dilution 1:400, Thermo Fisher Scientific), Hoechst 33342 (cat# H1399, dilution 1:1000, Thermo Fisher Scientific), Ly294002 (cat# PHZ1144, Sigma-Aldrich) and murine CXCL12 (cat# 250-20A, PeproTech, Rocky Hill, NJ).

Immunofluorescence microscopy

Cells were fixed with 4% paraformaldehyde for 20 min. After washing, the cells were permeabilized with Triton X-100 (0.1%) for 30 min. The Fc

receptors were blocked with goat serum to avoid non-specific binding. Immunolabeling with primary antibodies was performed with 30 min incubation at 4°C, followed by washing and incubation with species-specific fluorescence-labeled secondary antibodies or TRITC-Phalloidin (Thermo Fisher Scientific). The preparations were mounted with Vectashield (H-1000; Vector Laboratories, Burlingame, CA). The slides were analyzed via confocal microscopy (TCS SPE, Model DMI4000; Leica Microscopy, Wetzlar, Germany). Quantification of intensity fluorescence was performed using the program LAS AS lite 5.0 (Leica Microscopy).

Homing assays

Activated B cells from *Myo1e*^{+/+} or *Myo1e*^{-/-} mice were labeled with 0.1 µm or 0.6 µm CFSE (Thermo Fisher Scientific), respectively, or vice versa, in a complementary set of experiments. The cells were mixed at different ratios: 25%, 50% or 75% *Myo1e*^{+/+} B cells with the respective percentage of *Myo1e*^{-/-} B cells to complete 100%. The mixed suspensions of 1×10⁷ B cells were injected via the tail vein. The inguinal lymph nodes of a host wild-type mouse were inoculated for 1 h with CXCL12 (25 ng/ml) for the left node and with PBS for the right node. The host mouse was killed 2 h after inoculation. The blood, spleen and inguinal lymph nodes were extracted. The cells were recovered and measured using a BD LSR Fortessa flow cytometer and analyzed using FlowJo v10 software. For intravital microscopy, both inguinal lymph nodes were extracted to quantify the numbers of cells.

In vitro chemotaxis assays

For quantification of migration, a Zigmond chamber (Neuroprobe, Gaithersburg, MD) was used. Briefly, 1×10⁶ activated B lymphocytes from *Myo1e*^{+/+} and *Myo1e*^{-/-} mice were suspended in 0.5 ml RPMI 1640 supplemented with 10% fetal bovine serum and immediately plated onto glass coverslips. The glass coverslips were coated with fibronectin (2.5 µg/ml) (Sigma-Aldrich) in advance, and the cells were incubated for 30 min at 37°C and 5% CO₂ to allow their attachment. The coverslips, with the cells attached, were gently washed with PBS. One of the grooves in the Zigmond chamber was filled with supplemented medium (~70 µl) and the other with CXCL12 (2.5 µg/µl) dissolved in a supplemented medium. A baseline image was obtained at 10× magnification and digital images of the cells were taken every 30 s for 1 h, maintaining the temperature of the room between 35°C and 39°C. The migration tracks of at least 100 lymphocytes of *Myo1e*^{+/+} and *Myo1e*^{-/-} mice, in five independent experiments, were analyzed using ImageJ software (National Institutes of Health, Bethesda, MD) with chemotaxis and migration tool 2.0 (Ibidi, Martinsried, Munich, Germany) (Gorelik and Gautreau, 2014).

Adhesion assays

Polystyrene plates with 96 wells (Nalge Nunc International, Penfield, NY) were coated with hyaluronic acid (2.5 ng/ml) (Sigma-Aldrich), fibronectin (2.5 ng/ml) (Sigma-Aldrich), ICAM-1 Fc (2.5 ng/ml) (BioLegend), or poly-L-lysine (0.01%) (Sigma-Aldrich). The coating procedure was performed for 1 h at 37°C. After incubation, the plates were washed twice with PBS before adding 4×10⁵ panning-enriched B cells in 200 µl of RPMI 1640 per well. The cells adhered for 1 h at 37°C and the plates were washed with PBS. The cells were fixed for 10 min with 4% paraformaldehyde, before adding Crystal Violet (7.5 g/l Crystal Violet, 2.5 g/l NaCl, 1.57% formaldehyde, 50% methanol) for an additional 5 min. After that, the cells were solubilized with 10% SDS and the remaining dye in the plates was monitored at 540 nm (Multiskan Ascent; Thermo Fisher Scientific). Non-specific dye bound to empty wells was subtracted and the absolute binding was calculated. The absorbance was determined in four wells per condition.

Western blot analysis

B cells were lysed with RIPA buffer (20 mM Tris-HCl pH ~7.5, 150 mM NaCl, 1 mM EDTA, 1 mM EGTA, 1% Triton X-100, 1 µg/ml leupeptin, 10 µg/ml aprotinin and 1 mM PMSF) for 30 min at 4°C. The protein content was determined with a Modified Lowry Protein Assay Kit (Thermo Fisher Scientific). Proteins were separated via 12% SDS-PAGE at 85 V and 50 µg of each sample was analyzed. After electrophoresis separation, the proteins were transferred to a nitrocellulose membrane (Bio-Rad, Hercules, CA) at 120 V for 1.5 h. The membranes containing the transferred proteins were blocked for

30 min with 5% BSA. After blocking, the membranes were incubated 1 h at 37°C with specific antibodies. After washing with 0.01% TBS-Tween 20 (Sigma-Aldrich), the membranes were incubated with the respective secondary horseradish peroxidase (HRP)-labeled antibody. Finally, the blots were revealed with Western Blotting Chemiluminescence Luminol Reagent (Santa Cruz Biotechnology). Tubulin or actin was used as a loading control.

Intravital microscopy

The *Myo1e*^{+/+} host mouse was anesthetized by intraperitoneal injection of 12.5 mg/kg xylazine and 125 mg/kg ketamine hydrochloride (Sanofi, Mexico City, Mexico). Then, CXCL12 (25 ng/ml) was inoculated around the inguinal lymph node. One hour later, 1×10⁷ Hoechst 33342-labeled B cells were directly injected via the carotid artery. During the surgical procedure, it was necessary to keep the exposed tissue superfused with equilibrated warm physiological saline solution and to avoid contact with the vasculature or damaging the vessels. For the observation of the inguinal lymph node, we performed an incision in the abdominal cavity, then the skin was retracted and the connective tissue removed around the lymph node until the vasculature were observable (Sellers and Payne, 2011). The HEVs of the inguinal lymph node were recorded using an intravital upright microscope (Axioscope, Model A1; Zeiss, Oberkochen, Germany) with a 40× and 0.75 NA saline immersion objective. Videos and images were analyzed using ImageJ and Zen Blue Edition 2.5 software (Zeiss). The intravital experiments were recorded for 1 h. The diameter of the HEVs, the number of adherent cells, the number of transmigrated cells and the velocity of the cells were measured with ImageJ. Cell flux, blood flux, slow rolling and rolling were analyzed by Zen Blue Edition 2.5 software (Zeiss).

Pharmacological inhibition treatment

Ten million activated B cells were pretreated for 1 h with 20 μM LY294002 (Sigma-Aldrich) and stimulated with CXCL12 in RPMI-1640, supplemented with 5% fetal bovine serum or only supplemented medium. After PI3K inhibition and CXCL12 stimulation, the cells were used in the different experiments as indicated.

Co-immunoprecipitation assay

Protein extracts (500 μg) of resting or activated B cells were used. The lysates were centrifuged at 18,000 g for 30 min at 4°C. The supernatants were mixed with antibodies against Myo1e, FAK or CARMIL, using rabbit IgG or rat IgG as isotype controls. The supernatants were incubated overnight at 4°C with agitation. The complexes were precipitated with protein G-agarose (Life Technologies), maintaining the temperature at 4°C. Complexes were washed three times with RIPA buffer and boiled in Laemmli buffer. SDS-PAGE and western blotting were performed as previously indicated.

Statistical analysis

Data are presented as the arithmetic mean with s.d.; Student's *t*-test was used for evaluating statistical differences. A *P*-value <0.05 was considered statistically significant. The *P*-values are represented as **P*<0.05, ***P*<0.01 and ****P*<0.001, and the number of samples or cells (*n*) used is indicated in each figure legend.

Acknowledgements

We thank Dr Richard Flavell for the kind donation of the *Myo1e*^{-/-} mice; Dr Santiago Partida-Sanchez for his help to reinstate our colony of mice; Dr Hector Romero-Ramirez, Lenin Estudillo and Itze Cecilia Navarro Hernandez for technical support; and Ricardo Gaxiola-Centeno from the animal facility at CINVESTAV for taking care of the mice.

Competing interests

The authors declare no competing or financial interests.

Author contributions

Conceptualization: D.A.G.-P., L.S.-A.; Methodology: D.A.G.-P., L.S.-A., E.V., M.S.; Validation: D.A.G.-P., L.S.-A., M.S.; Formal analysis: D.A.G.-P.; Investigation: D.A.G.-P., E.V., L.S.-A.; Resources: D.A.G.-P., M.S., L.S.-A.; Data curation:

D.A.G.-P., E.V., L.S.-A.; Writing - original draft: D.A.G.-P., L.S.-A.; Writing - review & editing: D.A.G.-P., L.S.-A.; Visualization: D.A.G.-P., E.V., L.S.-A.; Supervision: L.S.-A., M.S.; Funding Acquisition: L.S.-A.

Funding

This work was supported Consejo Nacional de Ciencia y Tecnología [255053 to L.S.-A.; 305392 to D.A.G.-P.].

Supplementary information

Supplementary information available online at <http://jcs.biologists.org/lookup/doi/10.1242/jcs.235275.supplemental>

References

- Agelaki, S., Kallergi, G., Markomanolaki, C., Georgoulas, V. and Stournaras, C. (2007). FAK/PI3K activation controls actin reorganization and cell motility. *Cancer Res.* **67**, 977-986. doi:10.1159/000110458
- Ager, A. (2017). High endothelial venules and other blood vessels: critical regulators of lymphoid organ development and function. *Front. Immunol.* **8**, 45-67. doi:10.3389/fimmu.2017.00045
- Anderson, A. O. and Anderson, N. D. (1976). Lymphocyte emigration from high endothelial venules in rat lymph nodes. *Immunology* **31**, 731-748.
- Arthur, W. T., Quilliam, L. A. and Cooper, J. A. (2004). Rap1 promotes cell spreading by localizing Rac guanine nucleotide exchange factors. *J. Cell Biol.* **167**, 111-122. doi:10.1083/jcb.200404068
- Bargatze, R. F., Jutila, M. A. and Butcher, E. C. (1995). Distinct roles of L-selectin and integrins α4β7 and LFA-1 in lymphocyte homing to Peyer's patch-HEV in situ: the multistep model confirmed and refined. *Immunity* **3**, 99-108. doi:10.1016/1074-7613(95)90162-0
- Basit, A., Reutershan, J., Morris, M. A., Solga, M., Rose, C. E., Jr and Ley, K. (2006). ICAM-1 and LFA-1 play critical roles in LPS-induced neutrophil recruitment into the alveolar space. *Am. J. Physiol. Lung Cell. Mol. Physiol.* **291**, 200-207. doi:10.1152/ajplung.00346.2005
- Brandes, M., Legler, D. F., Spoerri, B., Schaeferli, P. and Moser, B. (2000). Activation-dependent modulation of B lymphocyte migration to chemokines. *Int. Immunol.* **12**, 1285-1292. doi:10.1093/intimm/12.9.1285
- Calalb, M. B., Zhang, X., Polte, T. R. and Hanks, S. K. (1996). Focal adhesion kinase Tyrosine-861 is a major site of phosphorylation by Src. *Biochem. Biophys. Res. Commun.* **228**, 662-668. doi:10.1006/bbrc.1996.1714
- Cannons, J. L., Qi, H., Lu, K. T., Dutta, M., Gomez-Rodriguez, J., Cheng, J., Wakeland, E. K., Germain, R. N. and Schwartzberg, P. L. (2010). Optimal germinal center responses require a multistage T Cell:B cell adhesion process involving integrins, SLAM-associated protein, and CD84. *Immunity* **32**, 253-265. doi:10.1016/j.immuni.2010.01.010
- Chang, F., Lemmon, C., Lietha, D., Eck, M. and Romer, L. (2011). Tyrosine phosphorylation of Rac1: a role in regulation of cell spreading. *PLoS ONE* **6**, 28587-28587. doi:10.1371/journal.pone.0028587
- Chayen, A. and Parkhouse, R. M. E. (1982). Preparation and properties of a cytotoxic monoclonal rat anti-mouse Thy-1 antibody. *J. Immunol. Methods* **49**, 17-23. doi:10.1016/0022-1759(82)90362-3
- Chen, C.-L., Wang, Y., Sesaki, H. and Iijima, M. (2012). Myosin I links PIP3 signaling to remodeling of the actin cytoskeleton in chemotaxis. *Sci. Signal.* **5**, 10-18. doi:10.1126/scisignal.2002446
- Chigaev, A. and Sklar, L. A. (2012). Aspects of VLA-4 and LFA-1 regulation that may contribute to rolling and firm adhesion. *Front. Immunol.* **3**, 242-256. doi:10.3389/fimmu.2012.00242
- Chuluyan, H. E. and Issekutz, A. C. (1993). VLA-4 integrin can mediate CD11/CD18-independent transendothelial migration of human monocytes. *J. Clin. Invest.* **92**, 2768-2777. doi:10.1172/JCI116895
- Chung, K.-J., Mitroulis, I., Wiessner, J. R., Zheng, Y. Y., Siegert, G., Sperandio, M. and Chavakis, T. (2014). A novel pathway of rapid TLR-triggered activation of integrin-dependent leukocyte adhesion that requires Rap1 GTPase. *Mol. Biol. Cell* **25**, 2948-2955. doi:10.1091/mbc.e14-04-0867
- Cossarizza, A., Chang, H.-D., Radbruch, A., Akdis, M., Andr , I., Annunziato, F., Bacher, P., Barnaba, V., Battistini, L., Bauer, W. M. et al. (2017). Guidelines for the use of flow cytometry and cell sorting in immunological studies. *Eur. J. Immunol.* **47**, 1584-1797. doi:10.1002/eji.201646632
- De Pascalis, C. and Etienne-Manneville, S. (2017). Single and collective cell migration: the mechanics of adhesions. *Mol. Biol. Cell* **28**, 1833-1846. doi:10.1091/mbc.e17-03-0134
- Doyle, A. D., Carvajal, N., Jin, A., Matsumoto, K. and Yamada, K. M. (2015). Local 3D matrix microenvironment regulates cell migration through spatiotemporal dynamics of contractility-dependent adhesions. *Nat. Commun.* **6**, 8720-8735. doi:10.1038/ncomms9720
- Engl, T., Relja, B., Marian, D., Blumenberg, C., M ller, I., Beecken, W.-D., Jones, J., Ringel, E. M., Bereiter-Hahn, J., Jonas, D. et al. (2006). CXCR4 chemokine receptor mediates prostate tumor cell adhesion through alpha5 and beta3 integrins. *Neoplasia* **8**, 290-301. doi:10.1593/neo.05694

- Francis, J., Meili, R., Del Alamo, J. C., Firtel, R. A. and Lasheras, J. C. (2016). Mechanics of adhesion dependent and independent neutrophil migration in three-dimensional extra-cellular matrices. *Biophys. J.* **110**, 512A. doi:10.1016/j.bpj.2015.11.2739
- Gerberick, G. F., Cruse, L. W., Miller, C. M., Sikorski, E. E. and Ridder, G. M. (1997). Selective modulation of T cell memory markers CD62L and CD44 on murine draining lymph node cells following allergen and irritant treatment. *Toxicol. Appl. Pharmacol.* **146**, 1-10. doi:10.1006/taap.1997.8218
- Girard, J.-P., Mousson, C. and Förster, R. (2012). HEVs, lymphatics and homeostatic immune cell trafficking in lymph nodes. *Nat. Rev. Immunol.* **12**, 762-773. doi:10.1038/nri3298
- Glodek, A. M., Le, Y., Dykxhoorn, D. M., Park, S.-Y., Mostoslavsky, G., Mulligan, R., Lieberman, J., Beggs, H. E., Honczarenko, M. and Silberstein, L. E. (2007). Focal adhesion kinase is required for CXCL12-induced chemotactic and pro-adhesive responses in hematopoietic precursor cells. *Leukemia* **21**, 1723-1732. doi:10.1038/sj.leu.2404769
- Goichberg, P., Kalinkovich, A., Borodovsky, N., Tesio, M., Petit, I., Nagler, A., Hardan, I. and Lapidot, T. (2006). cAMP-induced PKC ζ activation increases functional CXCR4 expression on human CD34⁺ hematopoietic progenitors. *Blood* **107**, 870-879. doi:10.1182/blood-2005-03-0941
- Gorelik, R. and Gautreau, A. (2014). Quantitative and unbiased analysis of directional persistence in cell migration. *Nat. Protoc.* **9**, 1931-1943. doi:10.1038/nprot.2014.131
- Hathcock, K. S., Hirano, H., Murakami, S. and Hodes, R. J. (1993). CD44 expression on activated B cells. Differential capacity for CD44-dependent binding to hyaluronic acid. *J. Immunol.* **151**, 6712-6722.
- Heim, J. B., Squirewell, E. J., Neu, A., Zocher, G., Somnidi-Damodaran, S., Wyles, S. P., Nikolova, E., Behrendt, N., Saunte, D. M., Lock-Andersen, J. et al. (2017). Myosin-1E interacts with FAK proline-rich region 1 to induce fibronectin-type matrix. *Proc. Natl Acad. Sci. USA* **114**, 3933-3938. doi:10.1073/pnas.1614894114
- Henderson, V., Smith, B., Burton, L. J., Randle, D., Morris, M. and Odero-Marah, V. A. (2015). Snail promotes cell migration through PI3K/AKT-dependent Rac1 activation as well as PI3K/AKT-independent pathways during prostate cancer progression. *Cell Adhes. Migr.* **9**, 255-264. doi:10.1080/19336918.2015.1013383
- Higuchi, M., Onishi, K., Kikuchi, C. and Gotoh, Y. (2008). Scaffolding function of PAK in the PDK1-Akt pathway. *Nat. Cell Biol.* **10**, 1356-1364. doi:10.1038/ncb1795
- Hood, J. D. and Cheresh, D. A. (2002). Role of integrins in cell invasion and migration. *Nat. Rev. Cancer* **2**, 91-100. doi:10.1038/nrc727
- Hu, Y.-L., Lu, S., Szeto, K. W., Sun, J., Wang, Y., Lasheras, J. C. and Chien, S. (2014). FAK and paxillin dynamics at focal adhesions in the protrusions of migrating cells. *Sci. Rep.* **4**, 6024-6039. doi:10.1038/srep06024
- Huang, X., Shen, Y., Zhang, Y., Wei, L., Lai, Y., Wu, J., Liu, X. and Liu, X. (2013). Rac1 mediates laminar shear stress-induced vascular endothelial cell migration. *Cell Adhes. Migr.* **7**, 472-478. doi:10.4161/cam.27171
- Kallergi, G., Agelaki, S., Markomanolaki, H., Georgoulas, V. and Stournaras, C. (2007). Activation of FAK/PI3K/Rac1 signaling controls actin reorganization and inhibits cell motility in human cancer cells. *Cell. Physiol. Biochem.* **20**, 977-986. doi:10.1159/000110458
- Kansas, G. S., Ley, K., Munro, J. M. and Tedder, T. F. (1993). Regulation of leukocyte rolling and adhesion to high endothelial venules through the cytoplasmic domain of L-selectin. *J. Exp. Med.* **177**, 833-838. doi:10.1084/jem.177.3.833
- Kim, D.-H. and Wirtz, D. (2013). Predicting how cells spread and migrate: focal adhesion size does matter. *Cell Adhes. Migr.* **7**, 293-296. doi:10.4161/cam.24804
- Kim, S. V., Mehal, W. Z., Dong, X., Heinrich, V., Pypaert, M., Mellman, I., Dembo, M., Mooseker, M. S., Wu, D. and Flavell, R. A. (2006). Modulation of cell adhesion and motility in the immune system by Myo1f. *Science* **314**, 136-139. doi:10.1126/science.1131920
- Kritikou, E. (2008). Recycling integrins. *Nat. Rev. Mol. Cell Biol.* **9**, 827-837. doi:10.1038/nrm2537
- Laffón, A., García-Vicuña, R., Humbría, A., Postigo, A. A., Corbí, A. L., De Landázuri, M. O. and Sánchez-Madrid, F. (1991). Upregulated expression and function of VLA-4 fibronectin receptors on human activated T cells in rheumatoid arthritis. *J. Clin. Invest.* **88**, 546-552. doi:10.1172/JCI115338
- Liang, Y., Niederstrasser, H., Edwards, M., Jackson, C. E. and Cooper, J. A. (2009). Distinct roles for CARM1 isoforms in cell migration. *Mol. Biol. Cell* **20**, 5290-5305. doi:10.1091/mbc.e08-10-1071
- Liu, Y., Dhali, S., Castro, A., Chan, A., Alamat, R. and Martins-Green, M. (2018). Insulin regulates multiple signaling pathways leading to monocyte/macrophage chemotaxis into the wound tissue. *Biol. Open* **7**, bio26187. doi:10.1242/bio.026187
- López-Ortega, O. and Santos-Argumedo, L. (2017). Myosin 1g contributes to CD44 adhesion protein and lipid rafts recycling and controls CD44 capping and cell migration in B lymphocytes. *Front. Immunol.* **8**, 1731. doi:10.3389/fimmu.2017.01731
- López-Ortega, O., Ovalle-García, E., Ortega-Blake, I., Antillón, A., Chávez-Munguía, B., Patiño-López, G., Fragoso-Soriano, R. and Santos-Argumedo, L. (2016). Myo1g is an active player in maintaining cell stiffness in B-lymphocytes. *Cytoskeleton* **73**, 258-268. doi:10.1002/cm.21299
- Ma, L., Rohatgi, R. and Kirschner, M. W. (1998). The Arp2/3 complex mediates actin polymerization induced by the small GTP-binding protein Cdc42. *Proc. Natl. Acad. Sci. USA* **95**, 15362-15367. doi:10.1073/pnas.95.26.15362
- Manevich, E., Grabovsky, V., Feiglson, S. W. and Alon, R. (2007). Talin 1 and Paxillin facilitate distinct steps in rapid VLA-4-mediated adhesion strengthening to vascular cell adhesion molecule 1. *J. Biol. Chem.* **282**, 25338-25348. doi:10.1074/jbc.M700089200
- Maravillas-Montero, J. L., Gillespie, P. G., Patiño-López, G., Shaw, S. and Santos-Argumedo, L. (2011). Myosin 1c participates in B cell cytoskeleton rearrangements, is recruited to the immunologic synapse, and contributes to antigen presentation. *J. Immunol.* **187**, 3053-3063. doi:10.4049/jimmunol.1004018
- Matsuoka, T., Yashiro, M., Nishioka, N., Hirakawa, K., Olden, K. and Roberts, J. D. (2012). PI3K/Akt signalling is required for the attachment and spreading, and growth in vivo of metastatic scirrhous gastric carcinoma. *Br. J. Cancer* **106**, 1535-1542. doi:10.1038/bjc.2012.107
- Mayor, R. and Etienne-Manneville, S. (2016). The front and rear of collective cell migration. *Nat. Rev. Mol. Cell Biol.* **17**, 97-109. doi:10.1038/nrm.2015.14
- Mesin, L., Ersching, J. and Victora, G. D. (2016). Germinal center B cell dynamics. *Immunity* **45**, 471-482. doi:10.1016/j.immuni.2016.09.001
- Mionnet, C., Sanos, S. L., Mondor, I., Jorquera, A., Laugier, J.-P., Germain, R. N. and Bajénoff, M. (2011). High endothelial venules as traffic control points maintaining lymphocyte population homeostasis in lymph nodes. *Blood* **118**, 6115-6122. doi:10.1182/blood-2011-07-367409
- Mitchison, T. J. and Cramer, L. P. (1996). Actin-based cell motility and cell locomotion. *Cell* **84**, 371-379. doi:10.1016/S0092-8674(00)81281-7
- Nader, G. P. F., Ezratty, E. J. and Gundersen, G. G. (2016). FAK, talin and PIPK γ regulate endocytosed integrin activation to polarize focal adhesion assembly. *Nat. Cell Biol.* **18**, 491-509. doi:10.1038/ncb3333
- Niba, E. T. E., Nagaya, H., Kanno, T., Tsuchiya, A., Gotoh, A., Tabata, C., Kuribayashi, K., Nakano, T. and Nishizaki, T. (2013). Crosstalk between PI3 Kinase/PDK1/Akt/Rac1 and Ras/Raf/MEK/ERK Pathways Downstream PDGF Receptor. *Cell. Physiol. Biochem.* **31**, 905-913. doi:10.1159/000350108
- Niggli, V., Djafarzadeh, S. and Keller, H. (1999). Stimulus-induced selective association of actin-associated proteins (α -Actinin) and protein kinase C isoforms with the cytoskeleton of human neutrophils. *Exp. Cell Res.* **250**, 558-568. doi:10.1006/excr.1999.4548
- Nolte, M. A., Hamann, A., Kraal, G. and Mebius, R. E. (2002). The strict regulation of lymphocyte migration to splenic white pulp does not involve common homing receptors. *Immunology* **106**, 299-307. doi:10.1046/j.1365-2567.2002.01443.x
- Okada, T. and Cyster, J. G. (2006). B cell migration and interactions in the early phase of antibody responses. *Curr. Opin. Immunol.* **18**, 278-285. doi:10.1016/j.coi.2006.02.005
- Onishi, K., Higuchi, M., Asakura, T., Masuyama, N. and Gotoh, Y. (2007). The PI3K-Akt pathway promotes microtubule stabilization in migrating fibroblasts. *Genes Cells* **12**, 535-546. doi:10.1111/j.1365-2443.2007.01071.x
- Oshero, N. and May, G. S. (2000). In vivo function of class I myosins. *Cell Motil. Cytoskelet.* **47**, 163-173. doi:10.1002/1097-0169(200011)47:3<163::AID-CM13>3.0.CO;2-U
- Paul, P., van den Hoorn, T., Jongsma, M. L. M., Bakker, M. J., Hengeveld, R., Janssen, L., Cresswell, P., Egan, D. A., van Ham, M., ten Brinke, A. et al. (2011). A genome-wide multidimensional RNAi screen reveals pathways controlling MHC class II antigen presentation. *Cell* **145**, 268-283. doi:10.1016/j.cell.2011.03.023
- Pereira, J. P., Kelly, L. M. and Cyster, J. G. (2010). Finding the right niche: B-cell migration in the early phases of T-dependent antibody responses. *Int. Immunol.* **22**, 413-419. doi:10.1093/intimm/dxq047
- Piedra-Quintero, Z. L., Serrano, C., Villegas-Sepúlveda, N., Maravillas-Montero, J. L., Romero-Ramírez, S., Shibayama, M., Medina-Contreras, O., Nava, P. and Santos-Argumedo, L. (2019). Myosin 1F regulates M1-polarization by stimulating intercellular adhesion in macrophages. *Front. Immunol.* **9**, 3118-3134. doi:10.3389/fimmu.2018.03118
- Qian, X., Li, G., Vass, W. C., Papageorge, A., Walker, R. C., Asnaghi, L., Steinbach, P. J., Tosato, G., Hunter, K. and Lowy, D. R. (2009). The Tensin-3 protein, including its SH2 domain, is phosphorylated by Src and contributes to tumorigenesis and metastasis. *Cancer Cell* **16**, 246-258. doi:10.1016/j.ccr.2009.07.031
- Sales, A., Ende, K., Diemer, J., Kyvik, A. R., Veciana, J., Ratera, I., Kemkemer, R., Spatz, J. P. and Guasch, J. (2019). Cell type-dependent integrin distribution in adhesion and migration responses on protein-coated microgrooved substrates. *ACS Omega* **4**, 1791-1800. doi:10.1021/acsomega.8b03608
- Salvermoser, M., Pick, R., Weckbach, L. T., Zehrer, A., Löh, P., Drechsler, M., Sperandio, M., Soehnlein, O. and Walzog, B. (2018). Myosin 1f is specifically required for neutrophil migration in 3D environments during acute inflammation. *Blood* **131**, 1887-1898. doi:10.1182/blood-2017-10-811851
- Santos-Argumedo, L., Kincaide, P. W., Partida-Sánchez, S. and Parkhouse, R. M. E. (1997). CD44-stimulated dendrite formation ('spreading') in activated B cells. *Immunology* **90**, 147-153. doi:10.1046/j.1365-2567.1997.00126.x

- Santos-Argumedo, L., Maravillas-Montero, J. L. and López-Ortega, O.** (2013). Class I myosins in B-cell physiology: functions in spreading, immune synapses, motility, and vesicular traffic. *Immunol. Rev.* **256**, 190-202. doi:10.1111/imr.12105
- Sellers, J. R.** (2000). Myosins: a diverse superfamily. *Biochim. Biophys. Acta Mol. Cell Res.* **1496**, 3-22. doi:10.1016/S0167-4889(00)00005-7
- Sellers, S. L. and Payne, G. W.** (2011). Intravital microscopy of the inguinal lymph node. *J. Vis. Exp.* 2551. doi:10.3791/2551
- Senbanjo, L. T. and Chellaiah, M. A.** (2017). CD44: a multifunctional cell surface adhesion receptor is a regulator of progression and metastasis of cancer cells. *Front. Cell Dev. Biol.* **5**, 18-28. doi:10.3389/fcell.2017.00018
- Smith, A., Bracke, M., Leitinger, B., Porter, J. C. and Hogg, N.** (2003). LFA-1-induced T cell migration on ICAM-1 involves regulation of MLCK-mediated attachment and ROCK-dependent detachment. *J. Cell Sci.* **116**, 3123-3133. doi:10.1242/jcs.00606
- Spaargaren, M., Beuling, E. A., Rurup, M. L., Meijer, H. P., Klok, M. D., Middendorp, S., Hendriks, R. W. and Pals, S. T.** (2003). The B cell antigen receptor controls integrin activity through Btk and PLC γ 2. *J. Exp. Med.* **198**, 1539-1550. doi:10.1084/jem.20011866
- Takabayashi, T., Takahashi, N., Okamoto, M., Yagi, H., Sato, M. and Fujieda, S.** (2009). Lipopolysaccharides increase the amount of CXCR4, and modulate the morphology and invasive activity of oral cancer cells in a CXCL12-dependent manner. *Oral Oncol.* **45**, 968-973. doi:10.1016/j.oraloncology.2009.06.006
- Tanaka, M., Kikuchi, T., Uno, H., Okita, K., Kitanishi-Yumura, T. and Yumura, S.** (2017). Turnover and flow of the cell membrane for cell migration. *Sci. Rep.* **7**, 12970-12977. doi:10.1038/s41598-017-13438-5
- Tanimura, S., Hashizume, J., Arichika, N., Watanabe, K., Ohyama, K., Takeda, K. and Kohno, M.** (2016). ERK signaling promotes cell motility by inducing the localization of myosin 1E to lamellipodial tips. *J. Cell Biol.* **214**, 475-489. doi:10.1083/jcb.201503123
- Thompson, R. F. and Langford, G. M.** (2002). Myosin superfamily evolutionary history. *Anat. Rec.* **268**, 276-289. doi:10.1002/ar.10160
- Vicente-Manzanares, M., Webb, D. J. and Horwitz, A. R.** (2005). Cell migration at a glance. *J. Cell Sci.* **118**, 4917-4919. doi:10.1242/jcs.02662
- Von Andrian, U. H.** (1996). Intravital microscopy of the peripheral lymph node microcirculation in mice. *Microcirculation* **3**, 287-300. doi:10.3109/10739689609148303
- Wakatsuki, T., Wysolmerski, R. B. and Elson, E. L.** (2003). Mechanics of cell spreading: role of myosin II. *J. Cell Sci.* **116**, 1617-1625. doi:10.1242/jcs.00340
- Walling, B. L. and Kim, M.** (2018). LFA-1 in T cell migration and differentiation. *Front. Immunol.* **9**, 952-965. doi:10.3389/fimmu.2018.00952
- Wang, Y., Li, D., Nurieva, R., Yang, J., Sen, M., Carreño, R., Lu, S., McIntyre, B. W., Mollrem, J. J., Legge, G. B. et al.** (2009). LFA-1 affinity regulation is necessary for the activation and proliferation of naive T cells. *J. Biol. Chem.* **284**, 12645-12653. doi:10.1074/jbc.M807207200
- Weninger, W., Ulfman, L. H., Cheng, G., Souchkova, N., Quackenbush, E. J., Lowe, J. B. and Von Andrian, U. H.** (2000). Specialized contributions by $\alpha(1,3)$ -Fucosyltransferase-IV and FucT-VII during leukocyte rolling in dermal microvessels. *Immunity* **12**, 665-676. doi:10.1016/S1074-7613(00)80217-4
- Wenzel, J., Ouderkirk, J. L., Krendel, M. and Lang, R.** (2015). Class I myosin Myo1e regulates TLR4-triggered macrophage spreading, chemokine release, and antigen presentation via MHC class II. *Eur. J. Immunol.* **45**, 225-237. doi:10.1002/eji.201444698
- Xue, F., Janzen, D. M. and Knecht, D. A.** (2010). Contribution of filopodia to cell migration: a mechanical link between protrusion and contraction. *Int. J. Cell Biol.* **2010**, 507821. doi:10.1155/2010/507821
- Yang, Y., Du, J., Hu, Z., Liu, J., Tian, Y., Zhu, Y., Wang, L. and Gu, L.** (2011). Activation of Rac1-PI3K/Akt is required for epidermal growth factor-induced PAK1 activation and cell migration in MDA-MB-231 breast cancer cells. *J. Biomed. Res.* **25**, 237-245. doi:10.1016/S1674-8301(11)60032-8
- Zhang, Y., Cao, F., Zhou, Y., Feng, Z., Sit, B., Krendel, M. and Yu, C.-H.** (2019). Tail domains of myosin-1e regulate phosphatidylinositol signaling and F-actin polymerization at the ventral layer of podosomes. *Mol. Biol. Cell* **30**, 622-635. doi:10.1091/mbc.E18-06-0398
- Zhu, G., Fan, Z., Ding, M., Zhang, H., Mu, L., Ding, Y., Zhang, Y., Jia, B., Chen, L., Chang, Z. et al.** (2015). An EGFR/PI3K/AKT axis promotes accumulation of the Rac1-GEF Tiam1 that is critical in EGFR-driven tumorigenesis. *Oncogene* **34**, 5971-5982. doi:10.1038/onc.2015.45
- Zimmermann, M., Rose, N., Lindner, J. M., Kim, H., Gonçalves, A. R., Callegari, I., Syedbasha, M., Kaufmann, L., Egli, A., Lindberg, R. L. P. et al.** (2019). Antigen extraction and B cell activation enable identification of rare membrane antigen specific human B cells. *Front. Immunol.* **10**, 829-844. doi:10.3389/fimmu.2019.00829

Supplementary Figure 1

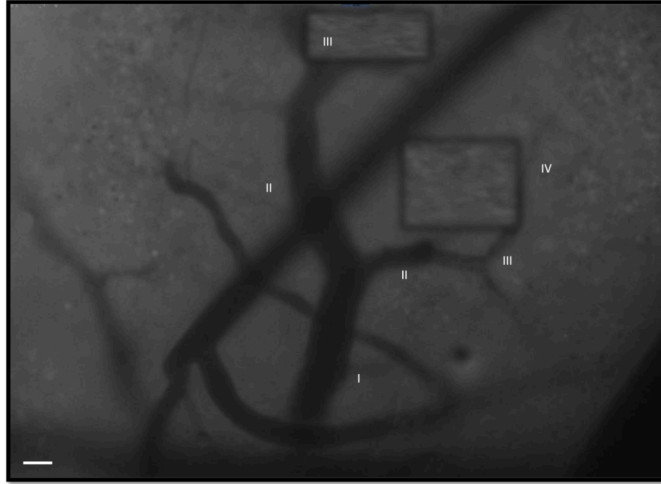


Fig. S1. HEV trees of the inguinal lymph node

Identification of the HEV with different diameters (from the narrow IV to wide I) in the inguinal lymph nodes of the WT host mice (Objective 40X). Scale bar: 25 μ m.

Supplementary Figure 2

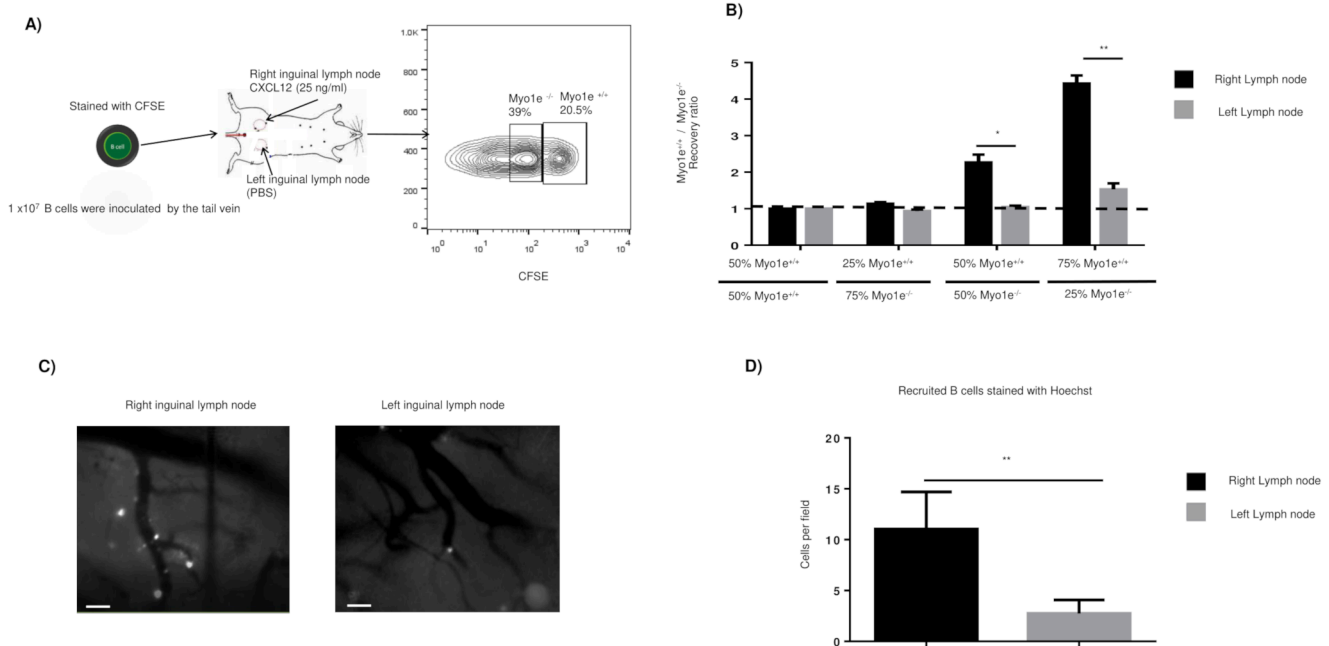


Fig. S2. *Myo1e* participates in the recruitment of B cells to the inguinal lymph node in response to CXCL12

A) Schematic representation of the injection of activated and CFSE-stained B cells from *Myo1e*^{+/+} and *Myo1e*^{-/-} mice. B) Adoptive transfer of activated B cells from *Myo1e*^{+/+} and *Myo1e*^{-/-} mice at different proportions (25%, 50%, and 75%) into the host mice; B cells were previously labeled with different concentrations of CFSE (0.6 μM for *Myo1e*^{+/+} and 0.1 μM for *Myo1e*^{-/-} or *vice versa*). One hour before B cell injection, the right inguinal lymph node was injected with CXCL12 and the left inguinal lymph node with PBS. Two hours later, the cells were recovered from each inguinal lymph node, and labeled B cells were identified and measured in each organ by flow cytometry. The recovery ratio was calculated by dividing the absolute numbers of *Myo1e*^{+/+} to the absolute numbers of *Myo1e*^{-/-} B cells; n=5. Data are mean ± SD. **p<0.01 *p<0.05. C). Representative images of activated B cells from *Myo1e*^{+/+} and *Myo1e*^{-/-} mice stained with CFSE and recruited to the right and left inguinal lymph node of the host mouse. (40x objective). Scale bars: 25 μm, n=5. D) Total of activated B cell (Hoechst33342-labeled) recruited to the right or left inguinal lymph node (independently if they were from *Myo1e*^{+/+} or *Myo1e*^{-/-}). The data are representative of 12 fields for each experiment; n=5. Data are mean ± SD **p<0.01.

Supplementary Figure 3

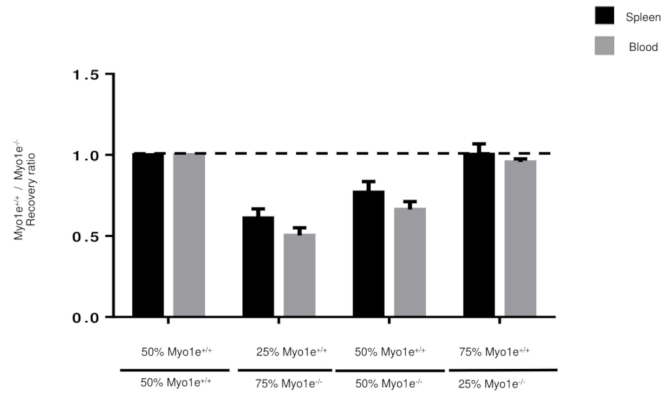


Fig. S3. Number of circulating B cells from Myo1e^{+/+} and Myo1e^{-/-} mice in the spleen and the blood

Adoptive transfer of activated B cells from Myo1e^{+/+} and Myo1e^{-/-} mice at different proportions (25%, 50%, and 75%) in the host mice. B cells were previously labeled with varying concentrations of CFSE (0.6 μ M Myo1e^{+/+} and 0.1 μ M Myo1e^{-/-} and vice versa). One hour before B cell injection, the right inguinal lymph node was inoculated with CXCL12 and the left inguinal lymph node with PBS. After 2 hours, the cells were recovered from the spleen and the blood and quantified. B cells were identified based on the CFSE-staining level, and the recovery ratio of each organ was measured by flow cytometry. The recovery ratio for each mix is shown in the graphics. The recovery ratio was calculated, dividing the absolute numbers of Myo1e^{+/+} between the total numbers of Myo1e^{-/-} B cells; n=5. Data are mean \pm SD.

Supplementary Figure 4

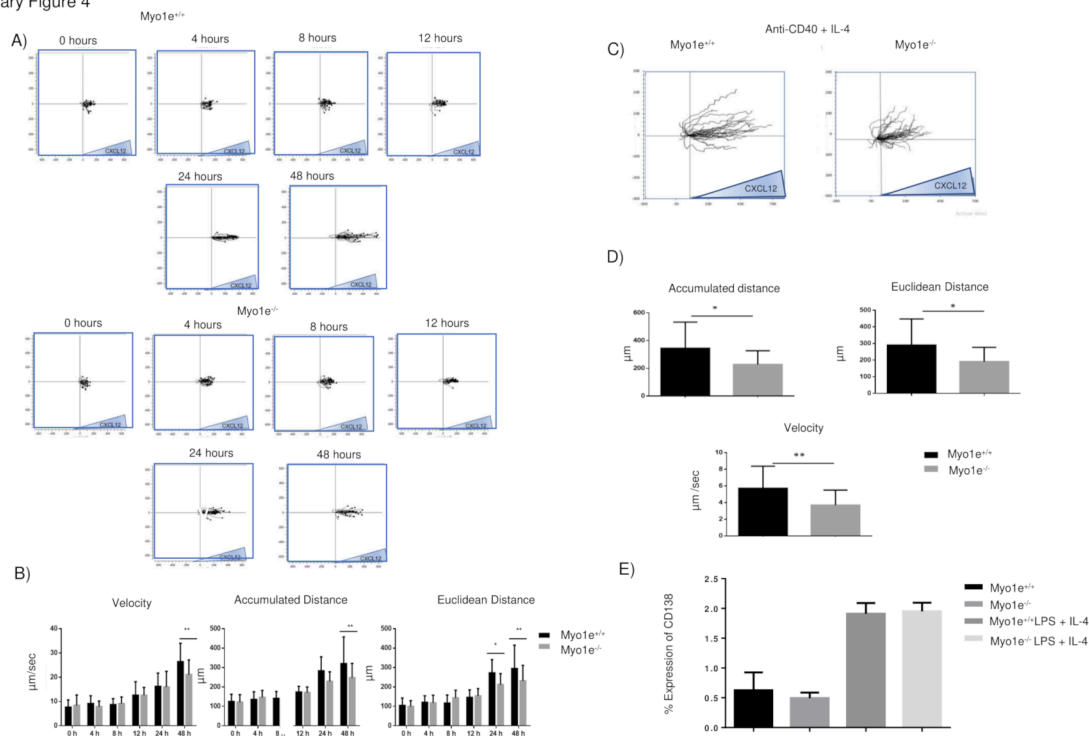


Fig S4. Kinetics of B cell migration in the absence of Myo1e; expression of CD138 by resting and 48 h LPS + IL-4 activated B cells.

A) LPS + IL-4 activated B cells at different times (0, 4, 8, 12, 24, and 48 hours) from of *Myo1e*^{+/+} and *Myo1e*^{-/-} mice were deposited in the Zigmond chamber under a CXCL12 gradient, and their migration was registered for 1 hour. Tracks of individual trajectories are presented in the plots. B) Measurements of the velocity, accumulated, and Euclidean distances in LPS + IL-4 activated B cells stimulated with CXCL12. Data are mean \pm SD. **p<0.01 *p<0.05. C) Activated (10 $\mu\text{g}/\text{ml}$ anti-CD40 and 10 U/ml of IL-4) B cells from of *Myo1e*^{+/+} and *Myo1e*^{-/-} mice were deposited in the Zigmond chamber under a CXCL12 gradient and registered for 1 hour. Tracks of individual trajectories are presented in the plots; n=3. D) Measurements of the velocity, accumulated, and Euclidean distances in anti-CD40 + IL-4 activated B cells stimulated with CXCL12; n=3. Data are mean \pm SD. **p<0.01 *p<0.05. E) Percentage of the expression of CD138 in resting and activated B cells from *Myo1e*^{+/+} and *Myo1e*^{-/-} mice; n=3. Data are mean \pm SD.

Supplementary Figure 5

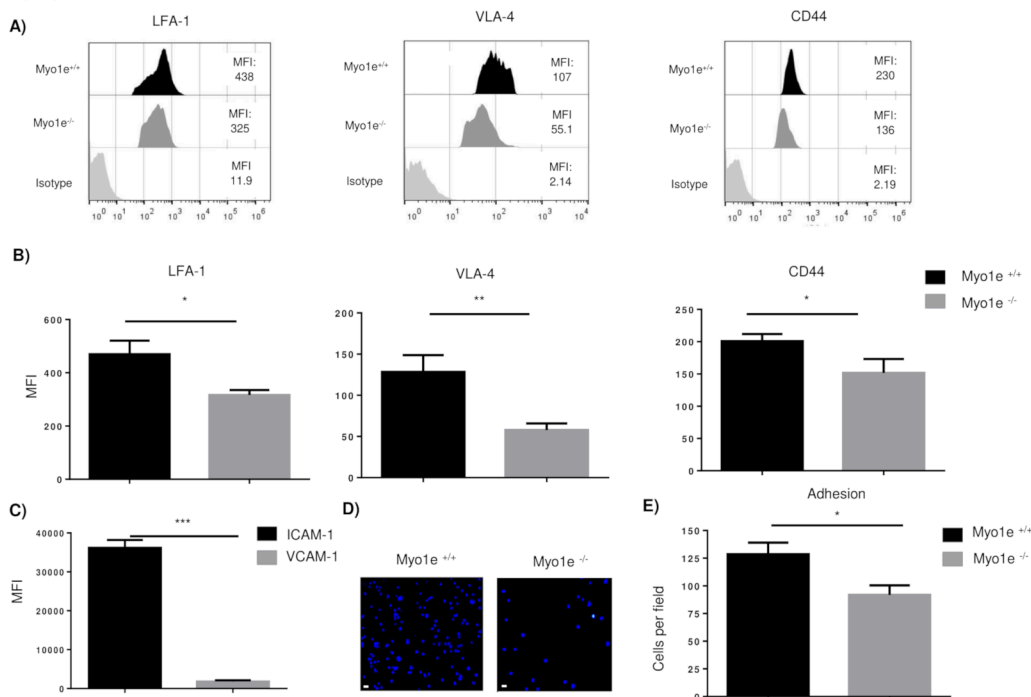


Fig. S5. Myo1e is required for cellular adhesion and allows efficient expression of adhesion molecules

A) Histograms of LFA-1, VLA-4, and CD44 on activated B cells from Myo1e^{+/+} and Myo1e^{-/-} mice; n=5 B) Mean fluorescence intensity of LFA-1, VLA-4, and CD44 in activated B cells from Myo1e^{+/+} and Myo1e^{-/-} mice; n=5. Data are presented as mean ± SD. **p<0.01 *p<0.05. C) Mean fluorescence intensity of ICAM-1 and VCAM-1 on the b-End3 cells; n=3. Data are mean ± SD, *** p<0.001 D) Representative images (10x objective) of activated B cells (stained with Hoechst 33342) from Myo1e^{+/+} and Myo1e^{-/-} mice. The cells were seeded over bEnd.3 cells, after four hours adhesion, unbound cells were washed out, and attached B cells were registered by epifluorescence microscopy. Scale bar 5 μm; n=3. E) Numbers of adherent Myo1e^{+/+} and Myo1e^{-/-} B cells, quantified in 12 fields; n=3. Data are mean ± SD. *p<0.05.

Supplementary Figure 6

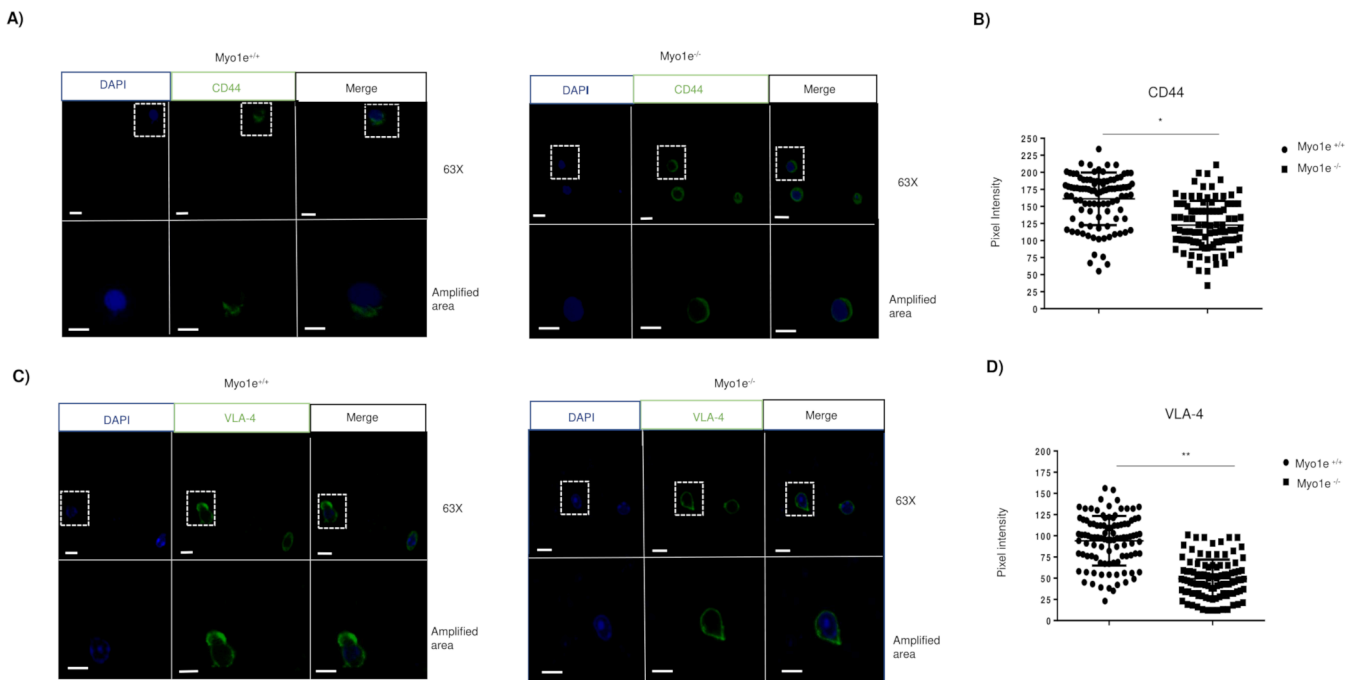


Fig. S6. The absence of *Myo1e* causes a reduction in the accumulation of CD44 and VLA-4 in the protrusions of membrane

A) Representatives images (63x objective) of activated (LPS + IL-4) B cells from of *Myo1e*^{+/+} and *Myo1e*^{-/-} mice, under a CXCL12 gradient. The cells were stained with anti-CD44 and DAPI. Scale bars 5 μm (Amplified area, zoom 2.5) B) The Pixel intensity of CD44 in the protrusion of membrane of activated B cells from of *Myo1e*^{+/+} and *Myo1e*^{-/-} mice was measured; n=3. Data are mean ± SD, *p<0.05 C) Representative images (63x objective) of activated (LPS + IL-4) B cells from of *Myo1e*^{+/+} and *Myo1e*^{-/-} mice, under a CXCL12 gradient. The cells were stained with anti-VLA-4 and DAPI. Scale bars 5 μm. (Amplified area, zoom 2.5) D) The pixel intensity of VLA-4 in the protrusion of membrane of activated B cells from of *Myo1e*^{+/+} and *Myo1e*^{-/-} mice; was measured; n=3. Data are mean ± SD, **p<0.01.

Supplementary Figure 7

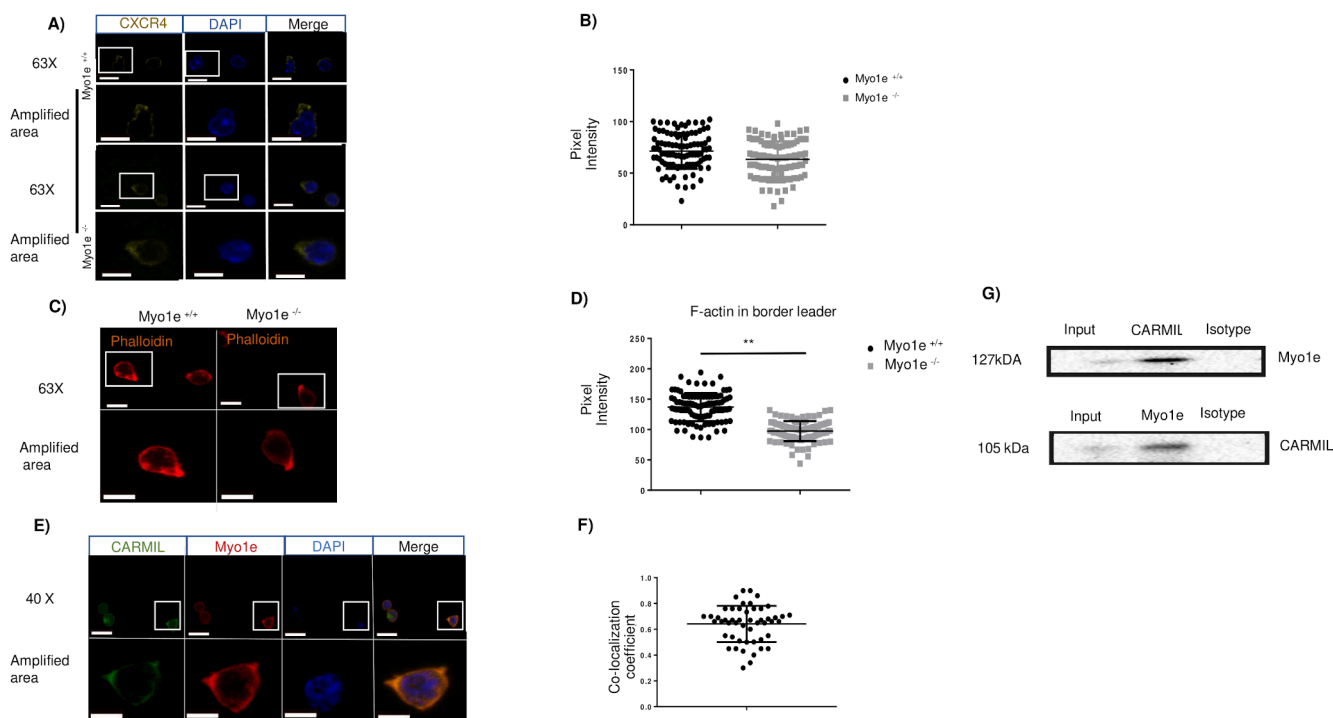


Fig. S7. The lack of Myo1e causes a reduction of F-actin in the border leader of B cells

A) Representative images (63x objective) of CXCR4 in the border-leader of Myo1e^{+/+} and Myo1e^{-/-} B cells stimulated by a gradient of CXCL12. Scale bars 5 μ m; (Amplified area, zoom 2.5); n=3. B) Quantification of the pixel intensity of CXCR4 in the protrusion of activated B cells from Myo1e^{+/+} and Myo1e^{-/-} mice. Data were acquired from 50 cells per experiment; n=3. Data are mean \pm SD. C) Representatives images (63x objective) of activated B cells from of Myo1e^{+/+} and Myo1e^{-/-} mice under a gradient of CXCL12. The cells were stained with TRITC-phalloidin (Red). Scale bars 5 μ m; (Amplified area, zoom 2.5) n=5. D) The pixel intensity of F-actin in the protrusions of the membrane was quantified; n=5. Data are mean \pm SD. **p<0.01. E) Representatives images (40x objective) of activated B cells from Myo1e^{+/+} mice stained with anti-Myo1e (Red), anti-CARMIL (Green), and DAPI (Blue). Scale bars 5 μ m; (Amplified area, zoom 2.5), n=3. F) Co-localization assays using Pearson's correlation index of Myo1e with CARMIL. The co-localization was measured in 50 cells per experiment; n=3. Data are mean \pm SD. G) Co-immunoprecipitation of Myo1e with CARMIL in activated B cells from Myo1e^{+/+} mice, n=3.



Movie 1

Activated Myo1e^{+/+} B cells running through the venules of an inguinal lymph node previously (1 h) inoculated with PBS. (40x objective).



Movie 2

Activated Myo1e^{-/-} B cells running through the venules of an inguinal lymph node previously (1 h) inoculated with PBS. (40x objective).



Movie 3

Activated $Myo1e^{+/+}$ B cells running through the venules of an inguinal lymph node previously (1 h) inoculated with CXCL12 (25 ng/ml). (40x objective).



Movie 4

Activated $Myo1e^{-/-}$ B cells running through the venules of an inguinal lymph node previously (1 h) inoculated with CXCL12 (25 ng/ml). (40x objective).